DIGITAL IMAGE DEBLURRING BY NONLINEAR HOMOMORPHIC FILTERING

Thomas Michael Cannon

Utah University

Prepared for:

Defense Advanced Research Projects Agency

August 1974

UNCLASSIFIED

SECURITY CLASSIFICATION OF THIS PAGE *(When Data Entered)*

REPORT DOCUMENTATION PAGE		READ INSTRUCTIONS BEFORE COMPLETING FORM
1. REPORT NUMBER UTEC-CSc-74-091	2. GOVT ACCESSION NO.	3. RECIPIENT'S CATALOG NUMBER AD/A-002735
4. TITLE *(and Subtitle)* DIGITAL IMAGE DEBLURRING BY NONLINEAR HOMOMORPHIC FILTERING		5. TYPE OF REPORT & PERIOD COVERED Technical Report 6. PERFORMING ORG. REPORT NUMBER
7. AUTHOR(s) Thomas Michael Cannon		8. CONTRACT OR GRANT NUMBER(s) DAHC15-73-C-0363
9. PERFORMING ORGANIZATION NAME AND ADDRESS Computer Science Department University of Utah Salt Lake City, Utah 84112		10. PROGRAM ELEMENT, PROJECT, TASK AREA & WORK UNIT NUMBERS ARPA Order #2477
11. CONTROLLING OFFICE NAME AND ADDRESS Defense Advanced Research Projects Agency 1400 Wilson Blvd. Arlington, Virginia 22209		12. REPORT DATE August 1974 13. NUMBER OF PAGES 93
14. MONITORING AGENCY NAME & ADDRESS *(if different from Controlling Office)*		15. SECURITY CLASS. *(of this report)* UNCLASSIFIED 15a. DECLASSIFICATION/DOWNGRADING SCHEDULE

16. DISTRIBUTION STATEMENT *(of this Report)*

This document has been approved for public release and sale; its distribution is unlimited.

17. DISTRIBUTION STATEMENT *(of the abstract entered in Block 20, if different from Report)*

18. SUPPLEMENTARY NOTES

19. KEY WORDS *(Continue on reverse side if necessary and identify by block number)*

linear system, convolution, deconvolution, deblurring, power spectrum, image restoration, Fourier transform, nonlinear, cepstrum

20. ABSTRACT *(Continue on reverse side if necessary and identify by block number)*

This report is concerned with the digital estimation of the frequency response of a two-dimensional linear system through which images have been passed and blurred. Almost no a priori knowledge concerning the system is required, and only one blurred image is necessary for a successful estimation. For those blurs that have phase reversals, such as motion blurs and out-of-focus blurs, a simple method of calculating the correct phase has been developed. A nonlinear homomorphic restoration system is developed

DD FORM 1 JAN 73 1473 EDITION OF 1 NOV 65 IS OBSOLETE

UNCLASSIFIED

SECURITY CLASSIFICATION OF THIS PAGE *(When Data Entered)*

20. Abstract (Continued)

and demonstrated on various types of blurred images. An image may be restored by filtering either the intensity version or the density version of the image. The latter not only insures a positive result but also permits simultaneous deblurring and contrast enhancement. The restoration procedure consumes only a modest amount of computation time.

DIGITAL IMAGE DEBLURRING BY NONLINEAR HOMOMORPHIC FILTERING

by

Thomas Michael Cannon

August 1974 UTEC-CSc-74-091

This research was supported by the Advanced Research Projects Agency of the Department of Defense under Contract No. DAHC15-73-C-0363 and Contract No. F30602-70-C-0300.

TABLE OF CONTENTS

List of Figures

LIST OF DIAGRAMS

ABSTRACT†

This report is concerned with the digital estimation of the frequency response of a two-dimensional linear system through which images have been passed and blurred. Almost no a priori knowledge concerning the system is required, and only one blurred image is necessary for a successful estimation. For those blurs that have phase reversals, such as motion blurs and out-of-focus blurs, a simple method of calculating the correct phase has been developed. A nonlinear homomorphic restoration system is developed and demonstrated on various types of blurred images. An image may be restored by filtering either the intensity version or the density version of the image. The latter not only insures a positive result but also permits simultaneous deblurring and contrast enhancement. The restoration procedure consumes only a modest amount of computation time.

---

† This report reproduces a dissertation of the same title submitted to the Department of Electrical Engineering, University of Utah, in partial fulfillment of the requirements for the degree of Doctor of Philosophy.

CHAPTER 1

Problem Description

1.1 Introduction

Two-dimensional imagery, be it digital, electronic, or photographic, has found use in many areas of modern endeavor. For example, many scientific space vehicles and other high-altitude craft rely heavily on two-dimensional data as a means of obtaining information. Objects of study may range from Nix Olympica on Mars to marijuana fields in New Mexico to sections of a submarine hull in a Moscow steel yard. Aerial photography may also be used for geographic purposes, mensuration, conservation studies, and weather prediction. More down-to-earth uses of two-dimensional data include conventional medical X-rays (radiographs), angiograms, stress photography, and flash radiography, to name but a few. There are also many signals that are not pictorial in nature but are nevertheless two-dimensional, such as those obtained from many types of radar and sonar as well as some forms of geophysical seismic soundings.

All of the above signals, though perhaps not explicitly digital in nature, can be represented as such in a digital computer. This permits one to apply a variety of digital techniques to the data to achieve any of a wide range of goals such as image enhancement, data

compression, scene analysis, or restoration. It is the last of these operations which is explored in this thesis.

The problem associated with restoration is the following: the data we have been given has been blurred in some way; further, the exact type or extent of blur is not known, but must be determined from the blurred image itself. The goal is to remove this blurring degradation from the image.

1.2 Mathematical Model

It will be assumed that the cause of the blurring can be modeled as a linear system. The image may be considered a function of intensity vs the spatial dimensions x and y, as shown in Diagram 1.

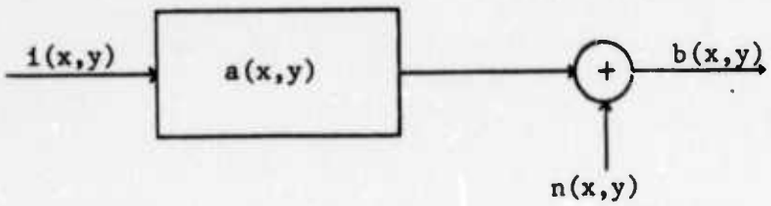

Diagram 1

a(x,y) is the impulse response, or point-spread function, of the system, and is assumed to be unknown. All noise, n(x,y), is modeled as additive, although this may not always reflect reality (film-grain noise being a prime example). A discussion of the characteristics of the noise will be presented in Chapter 4.

The relation between the input and output is that of convolution, namely:

$$b(x,y) = \int\int i(x-x_o, y-y_o)\, a(x_o, y_o)\, dx_o dy_o + n(x,y) \dagger \qquad (1.1)$$

Or

$$b(x,y) = i(x,y) \circledast a(x,y) + n(x,y) \qquad (1.2)$$

$a(x,y)$ is commonly referred to as the kernel. In this particular problem, we are given $b(x,y)$ and must estimate $i(x,y)$ having very little knowledge of the blurring system, $a(x,y)$, or the noise, $n(x,y)$.

It has been established that the Fourier integral transform maps convolution into multiplication (and addition into addition), hence:

$$\mathcal{F}\{b(x,y)\} = \mathcal{F}\{i(x,y)\} \cdot \mathcal{F}\{a(x,y)\} + \mathcal{F}\{n(x,y)\} \qquad (1.3)$$

where

$$G(u,v) = \mathcal{F}\{g(x,y)\} = \int\int g(x,y) \exp[-j(ux, vy)]\, dxdy \qquad (1.4)$$

The Fourier transform domain is commonly referred to as the frequency domain. In view of this, the author finds it much simpler and mnemonically more pleasing to use f instead of u,v. Equation 1.3 can then be written as:

$$B(f) = I(f) \cdot A(f) + N(f) \qquad (1.5)$$

If the noise were negligible, and $A(f)$ were known, this could be written as

---

† For a discussion of the discrete representation of these relationships, as well as the continuous forms shown here, the reader is referred to references [1] and [2]. Unless specified otherwise, limits of integration are from $-\infty$ to $+\infty$.

$$I(f) = B(f)/A(f) \tag{1.6}$$

However, it is well known that we are not so fortunate when considering actual problems.

If i(x,y) and n(x,y) are viewed as random processes, then a final relationship can be written that will prove most helpful, namely the relationship between the power spectra of the input and output of the blurring system:

$$P_i(f)|A(f)|^2 + P_n(f) = P_b(f) \tag{1.7}$$

where $P_b(f)$ is the power spectrum of the signal b(x,y), etc.

In choosing this blurring model, the case of the spatially varying blur has been precluded. The blurs considered here must be isoplanatic - for example, each portion of the image must be equally out-of-focus. There are three major blurs that can be modeled by such a system, and these are outlined below.

1.3 Camera Motion Blur

Subjecting a point of light to camera motion produces a streak in the resulting picture. Plotting intensity as a function of x and y gives this streak the appearance of a rectangular wall. The frequency response, A(f), is the Fourier transform of this rectangle and has the form of sin(x)/x in the direction of the blur, and is constant in the direction perpendicular to the blur. The magnitude of A(f) (or

modulation transfer function) is shown in Figure 1.1 on a db scale. Alternate lobes are negative, and hence have a phase of π radians associated with them. So not only are the higher frequencies of a motion-blurred image attenuated, but some experience a sign change also.

1.4 Out-of-Focus Blur

The point-spread function of an out-of-focus lens system can be approximated by a cylinder; that is, each point of light in the image is spread out evenly over a circular area. This is illustrated in Diagram 2.

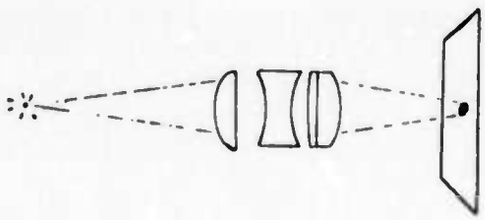

Diagram 2

Although the true point-spread function is actually related to the Fourier transform of the aperture of the lens system[3], the cylindrical approximation is a good one and is also mathematically tractable. The frequency response of the system is of the form $J_1(r)/r$, where $J_1(r)$ is a Bessel function of the first kind, order one, as shown in Figure 1.1. An image passed through this system will not only have its higher frequencies suppressed, but, due to the negative lobes of A(f), some frequencies will undergo a phase shift of

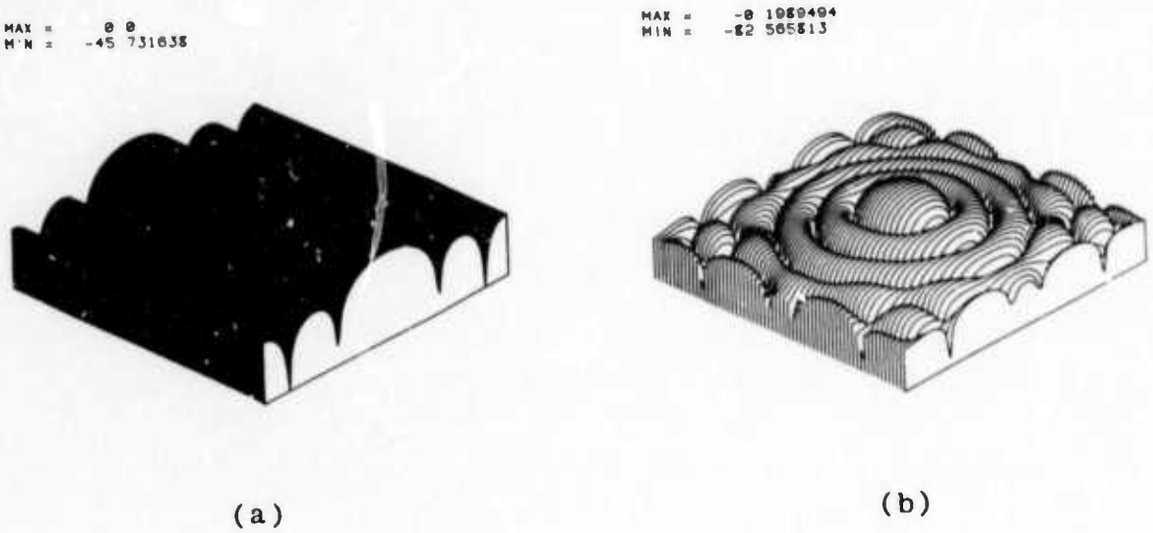

(a) (b)

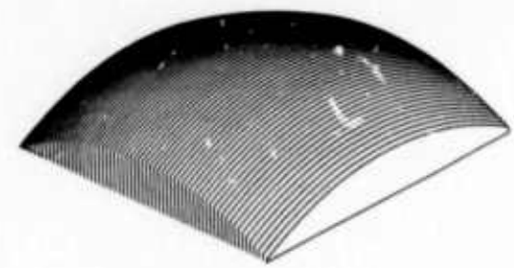

(c)

Figure 1.1

The modulation transfer functions (on a db scale) of

(a) horizontal motion blur
(b) out-of-focus blur
(c) atmospheric turbulence blur

π radians (as was also pointed out in the case of motion blur).

1.5 Turbulence Blur

A third type of blur that can be modeled by a linear system is that resulting from atmospheric turbulence. To explain the model of the point-spread function let us consider a real-world situation in which a star is being viewed from a terrestrial observation point. Were the star being viewed through an optically uniform medium, it would appear to shine with constant intensity. However, since the atmosphere is not thermally uniform, its index of refraction varies as a function of time and position; hence the rays of light from a celestial object are refracted varying amounts. The resulting twinkling is well known.

A point of light coming through the atmosphere assumes a gaussian distribution of the form $\exp(-kr^2)$ when averaged over time[17]. This explains why terrestrial photographs of stars seldom depict sharp images, but instead indistinct fuzzy blobs. The frequency response is also gaussian (see Appendix D) so the blurred image suffers no phase shifts but simply an attenuation of higher frequencies, as shown in Figure 1.1.

1.6 Problems Involved in Restoration

The immediate problem in restoration is the identification of A(f), the frequency response of the blurring system. But even after A(f) has been identified, other problems remain. It was noted previously that if the Fourier transform of the blurred image, B(f), and the transform of the system response, A(f), were identified, it might be possible to find the original image by a simple division, i.e.

$$B(f) = I(f) \cdot A(f) \tag{1.8}$$

$$I(f) = B(f)/A(f) \tag{1.9}$$

It is commonly understood that this is not usually possible, or at least not optimal, for a variety of reasons. One is that for some values of f, A(f) may be zero, which happens to occur in the case of motion blur and out-of-focus blur. Another difficulty results from the addition of random noise to the blurred image, which precludes a perfect restoration. One of the effects of the filters used to restore a blurred image is to boost high frequency power in the image; any noise residing in those frequencies will also be amplified, and may easily dominate the restoration. The consequences of ignoring this ill-conditioned nature of the restoration system will be illustrated in Chapter 3.

The above discussion assumes that an explicit knowledge of A(f) (or a(x,y)) is available. Most researchers assume that this knowledge

is known a priori, even though such a case is the exception rather than the rule. This dissertation is restricted to those blurs for which a(x,y) is unknown. This portion of the deblurring problem has two parts; one is the estimation of the blur magnitude, and the second that of determining the associated phase. The problem of phase estimation has remained extraordinarily difficult[5], even though much of the groundwork has been laid for determining the magnitude of a linear blur[4]. A solution to the phase problem (for the types of blurs discussed above) is presented in the next chapter.

There remain two final problems in digital image restoration. The first is that the process is just that - digital. It has been explained that the blurring process is one of convolution; the deblurring process is also, but a problem arises from the fact that the deblurring kernel, which is in some way related to the convolutional inverse of a(x,y), may have infinite extent. This is no obstacle to a mathematician but does pose serious problems to the finite capacity of a digital computer. The methods of terminating gracefully an infinite computation will be discussed later.

The final problem in image restoration is easily overlooked. The original image (which is a representation of the light intensity of a scene, blurred or otherwise), is everywhere positive. There is no assurance, however, that it will remain so after passage through a linear deblurring system. Negative values of intensity in a restored

image have, of course, no physical meaning. This problem has been the focal point of much research in recent years, an excellent survey of which has been prepared by Andrews[20]. Most of the present methods, however, require an excessive amount of computation time. The present author's method for overcoming the problem will be presented in Chapter 3.

CHAPTER 2

Restoration By Power Spectrum Equalization

2.1 A Nonlinear Homomorphic Restoration System

Chapter 1 introduced the mathematical model of the blurring system, describing it as a linear system with additive noise. The blurred output, b(x,y), of this system will be restored by passing it through the nonlinear system shown in Diagram 3.

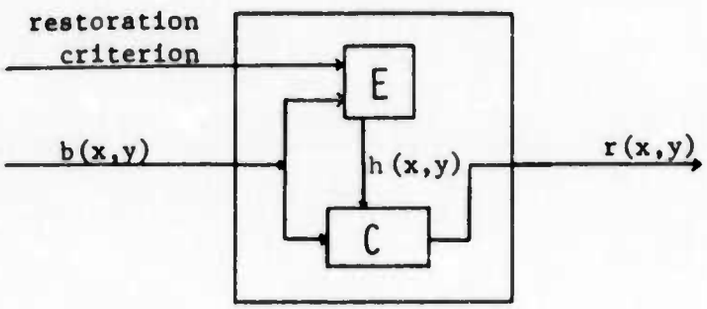

Diagram 3

E is an estimator which has as inputs the blurred image itself and a restoration criterion. From these two inputs a restoration kernel is generated which, when convolved with the blurred image, produces a restored image satisfying the given criterion. The restoration kernel, h(x,y), is re-estimated for each new input to the system. C is simply a two-dimensional convolver, which convolves this kernel with the blurred image.

The restoration system is termed homomorphic because it has the ability to map several different blurred versions of an image back into that same image. This ability is a benefit of the nonlinear nature of the restoration system. The task of the estimator is therefore especially difficult, as it must determine the nature of the blurring system from an individual blurred image submitted for restoration.

2.2 The Restoration Criterion of Power Spectrum Equalization

Many constraints may be placed on h(x,y) to produce a restored image, r(x,y). One restoration criterion might consist of constraining h(x,y) such that the expected mean squared difference between the restored image, r(x,y), and the original, undegraded image, i(x,y), would be minimized. This is a reasonable criterion and is discussed fully in Chapter 3. A mathematically simpler approach can be established from the discussion in Chapter 1 concerning power spectra. Let h(x,y) be constrained such that

$$P_s(f)|H(f)|^2 = P_r(f) = P_i(f) \qquad (2.1)$$

This relationship states that h(x,y) will be constrained so that the power spectrum of the restored image will be equal to the power spectrum of the original image. This is a reasonable thing to demand. It means that the distribution of power according to frequency in the restored image will be set to what it originally was before the

blurring occurred. This approach is an adaptation of the nonlinear homomorphic filtering developed by Stockham[6],[18],[19] and later expanded by Cole[4] to two dimensions. Their method utilizes the average log spectrum, which is somewhat different than the power spectrum. (See Appendix A, which compares the two.) Solving equation 2.1 for $|H(f)|$ yields:

$$|H(f)| = [P_i(f)/P_g(f)]^{1/2} \tag{2.2}$$

Or, using the fact that

$$P_g(f) = P_i(f)|A(f)|^2 + P_N(f) \tag{1.7}$$

we can write

$$|H(f)| = \{P_i(f)/[P_i(f)|A(f)|^2 + P_N(f)]\}^{1/2} \tag{2.3}$$

To obtain $P_i(f)$, the ergodic hypothesis is invoked to permit the estimation of the power spectrum from a scene that is considered to be a member of the statistical ensemble to which $i(x,y)$ belongs (Appendix A). The justification for this is illustrated in Figure 2.2, which shows the similarity of the power spectra of the images of Figure 2.1.

It is interesting to note that for those frequencies in which the noise power is small relative to signal power the following holds:

$$|H(f)| \propto 1/|A(f)| \tag{2.4}$$

The homomorphic filter attempts to correct for the effects of the magnitude of $A(f)$, and does so with no knowledge of the phase of the blurring system. Therefore, $H(f)$ must be further constrained to take

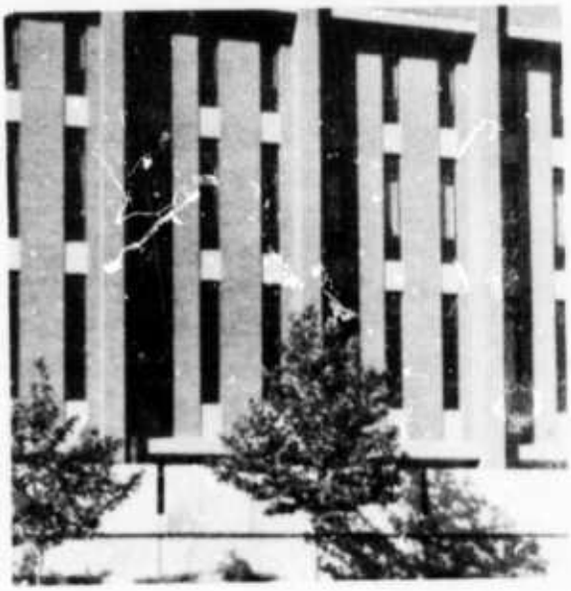

(a)

(b)

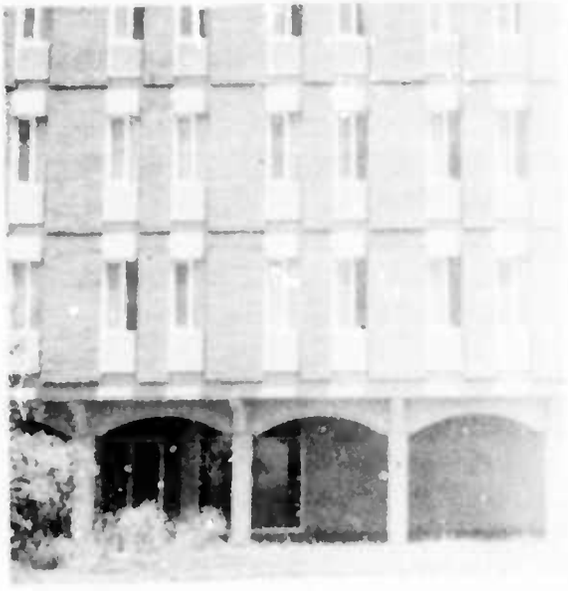

(c)

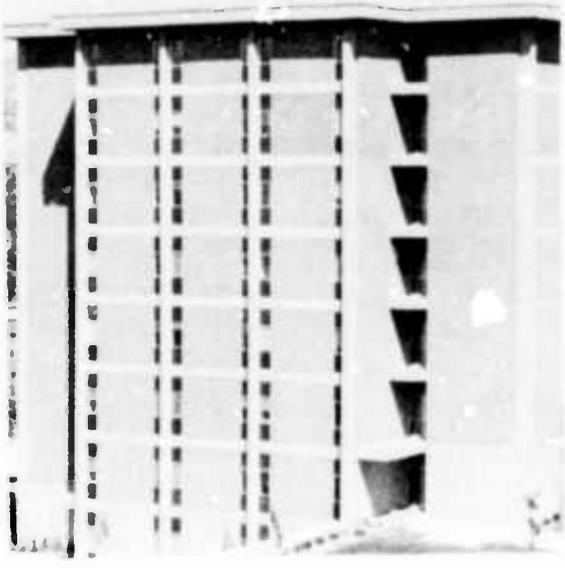

(d)

Figure 2.1
Four statistically similar digital images.

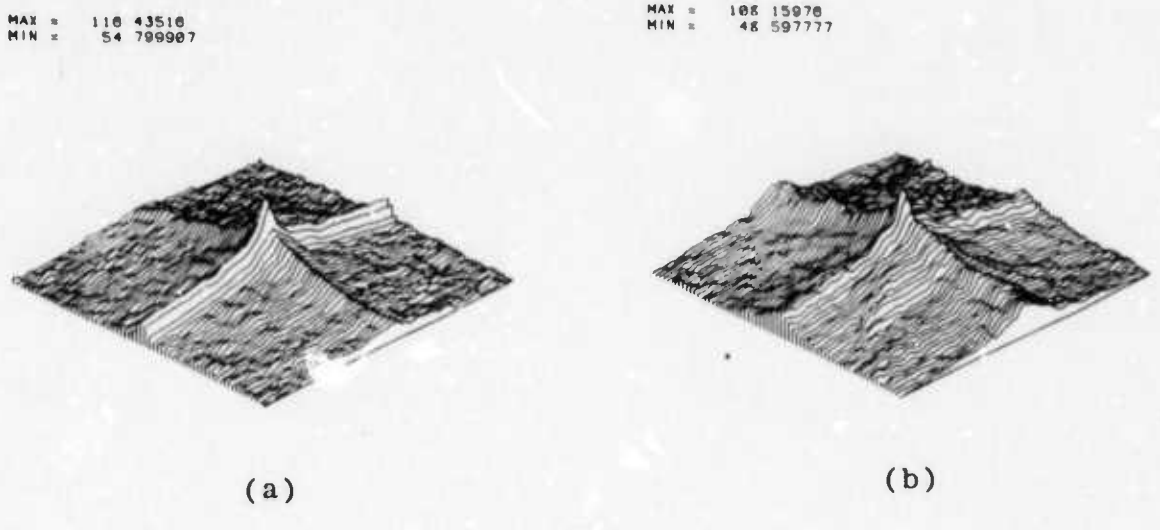

Figure 2.2
The power spectra of the images of Figure 2.1

into account the phase of the blur. In general, the determination of the phase of a blur is a difficult problem. One might ask if an averaging scheme similar to that used to obtain the power spectrum of an image (see Appendix A) could be used to obtain the phase information needed by H(f), perhaps through a relationship similar to that of equation 2.2. Unfortunately, this must be answered in the negative. The reader is refered to work by Cole[4] and McGlamery[5], who have shown that the phase does not converge to a statistically meaningful quantity. The author therefore proposes a different scheme based on the nature of the power spectra of both clear and blurred images. Figure 2.3 shows the power spectra of two clear images and also the spectra of the same two images photographed out-of-focus. The effect of blurring is strikingly obvious, as one can see the imprint of $|A(f)|$ on $P_I(f)$. In Figure 2.3d the effect of adding the power in the noise, $P_N(f)$, is also apparent, for the signal power drops well below the noise power at higher frequencies.

2.3 Phase Estimation by the Zero Crossing Technique

One characteristic common to both these power spectra and almost all others is that signal power is very high relative to noise in the lower frequencies. On the basis of this fact and equation 2.4 it can be concluded that $|H(f)|$ will approximately equal $1/|A(f)|$ at these frequencies. Figure 2.4 shows this to be true. $P_I(f)$ was estimated from the image of Figure 2.2a.

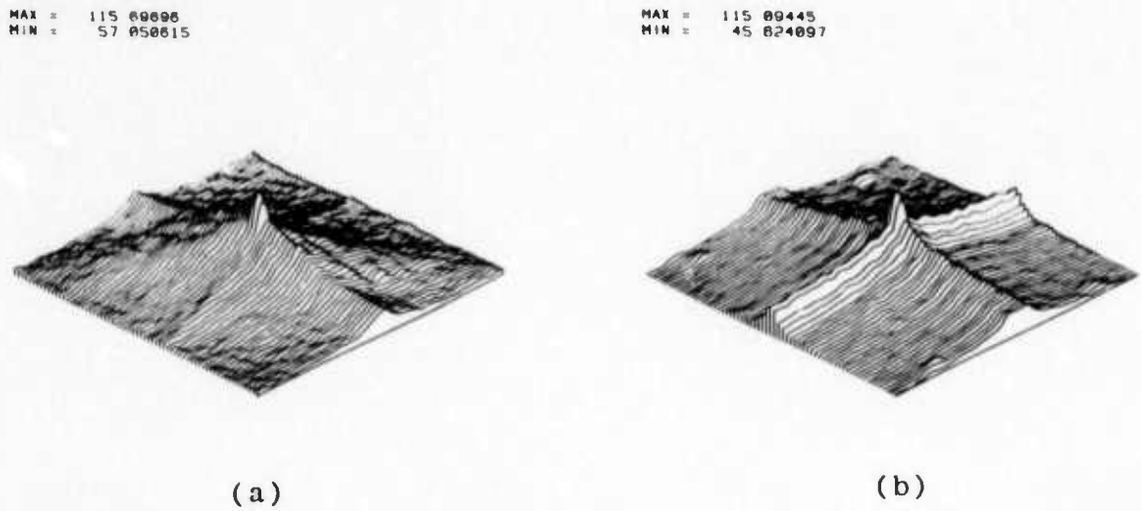

Figure 2.3

(a) and (b): The power spectra of two in-focus images.
(c) and (d): The power spectra of the same two images photographed out-of-focus.

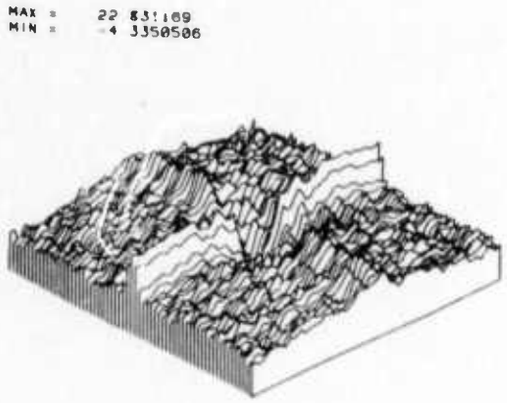

(a)

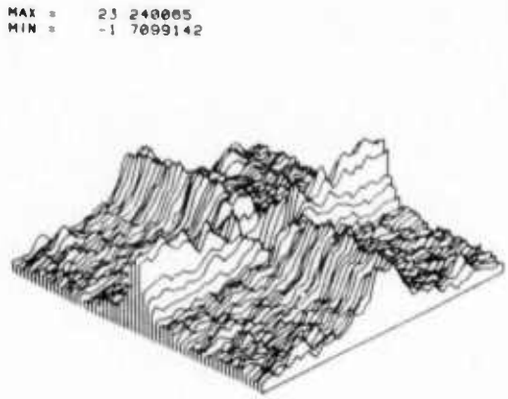

(b)

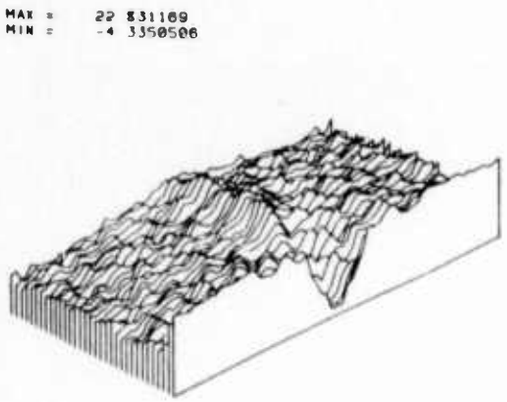

(c)

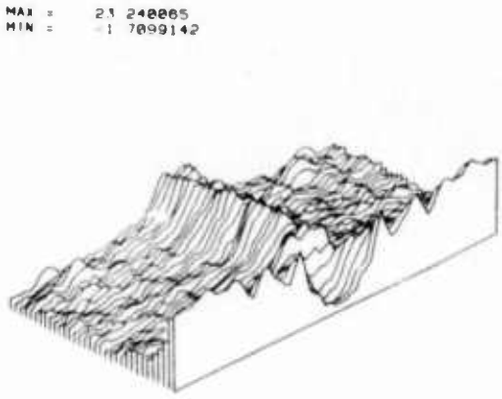

(d)

Figure 2.4

(a) and (b): The power spectra of Figures 2.3c and 2.3d minus a prototype power spectrum.
(c) and (d): Enlarged cross sections of the above spectra.

The fact that $1/|A(f)|$ is visible in the low-frequency regions of $|H(f)|$ is the key to the determination of the phase of the blur. An algorithm can be devised that searches for the first zero crossing of $|A(f)|$, and from that† generates the appropriate phase of 0 or π, depending on whether a certain lobe of $A(f)$ is positive or negative.

The task of determining the phase of a motion blur is similar to that of an out-of-focus blur except that the problem does not enjoy the circular symmetry of the out-of-focus blur. The basic notion is the same though, namely the searching of the low frequencies for zero crossings. The algorithm must know a priori, however, which of the three blurs described in Chapter 1 is present.

The present discussion on determination of phase may seem sketchy, which it is. The method described has some deficiencies, namely the inability to determine the direction of blur (in the case of motion blur) or the type of blur, i.e. out-of-focus, motion, or turbulence. A more sophisticated and powerful tool for phase estimation was therefore developed.

---

† Appendix C gives sufficient information on the spacing of the zero crossings and their relation to the point-spread function to implement the algorithm.

2.4 Phase Estimation by Cepstral Techniques

Although the concept of the cepstrum in one dimension has been understood for quite some time[7], it was only very recently that the properties of the two-dimensional cepstrum were investigated (Rom[8]). The cepstrum of an image, $i(x,y)$, which has Fourier transform $I(f)$, is defined as follows:

$$C(q) = \mathcal{F}(\log|I(f)|) \tag{2.5}$$

where q (quefrency) has the dimension of two-dimensional distance.

The properties of the two-dimensional cepstrum are similar to those of the one-dimensional cepstrum insofar as convolution is mapped into addition. This is demonstrable in our present problem, namely that of an image, $i(x,y)$, being convolutionally blurred by $a(x,y)$. Ignoring the effects of noise, the derivation is:

$$b(x,y) = i(x,y) \circledast a(x,y) \tag{2.6}$$

$$B(f) = I(f) \cdot A(f) \tag{2.7}$$

$$\log|B(f)| = \log|I(f)| + \log|A(f)| \tag{2.8}$$

$$\mathcal{F}(\log|B(f)|) = \mathcal{F}(\log|I(f)|) + \mathcal{F}(\log|A(f)|) \tag{2.9}$$

$$C_b(q) = C_i(q) + C_A(q) \tag{2.10}$$

One might well ask if $C_A(q)$, the cepstrum of the blur, is identifiable in $C_b(q)$, the cepstrum of the blurred image. Rom answers this in the affirmative, pointing out that spikes which are characteristic of $C_A(q)$ are apparent in $C_b(q)$. The origin of the

spikes is explained by the following. Suppose $a(x,y)$ is a rectangle of length α corresponding to a motion blur. $A(f)$ is then $\sin(\pi\alpha f)/(\pi\alpha f)$, which has zero crossings at intervals of $1/\alpha$. The logarithm of the magnitude of $A(f)$ will have periodic spikes of height $-\infty$ at these intervals of $1/\alpha$. The result of transforming this quantity will be a large negative spike a distance α from the origin in the cepstral domain. The location of the spike in the cepstrum indicates the direction of the motion blur as well as its length. The cepetrum of an out-of-focus blur is similar but circularly symmetric, owing to the circular symmetry of $J_1(r)/r$.

The presence of these spikes enables one to differentiate between out-of-focus and motion blur. The cepstrum of a turbulence blur lacks these characteristic spikes, which is an identifying feature in and of itself. The cepetrum not only identifies the type of blur but also reveals its extent. This information uniquely defines $a(x,y)$, the point-spread function of the blurring system. From $a(x,y)$ both the magnitude and phase components of the blur can be generated.

As equations 2.7 through 2.10 indicate, computing the cepstrum of even a small image is a time consuming operation. In view of the fact that our interest in the cepstrum arises only from the need to identify the blur and its phase, the author proposes the following shortcut. Equation 1.7, which describes the power spectrum of a blurred image, can be written as follows without the noise term:

$$P_g(f) = P_f(f)|A(f)|^2 \tag{2.11}$$

It is usual to take the logarithm of $P_g(f)$ in order to display it on a db scale. The Fourier transform of the logarithm of the power spectrum is termed the power cepstrum of the image:

$$\log P_g(f) = \log P_f(f) + 2\log|A(f)| \tag{2.12}$$

$$\mathcal{F}\{\log P_g(f)\} = \mathcal{F}\{\log P_f(f)\} + 2C_A(q) \tag{2.13}$$

As indicated by equation 2.13, the power cepstrum of a blurred image is the sum of the power cepstrum of the clear image and the cepstrum of the blurring system. It is this latter quantity which contains spikes characteristic of the nature of the blur.

Figure 2.5 presents the power spectrum and power cepstrum of an out-of-focus image. The power cepstrum has been clipped at zero and inverted to disclose the characteristic spikes of $C_A(q)$. The ring of spikes is clearly visible, especially in the overhead view. Figure 2.6 shows the power spectra and power cepstra of motion-blurred and turbulence-blurred images. The characteristic twin peaks of motion blur are easily recognized in the former, while no particular landmarks stand out in the latter.

This cepstral method of blur determination is independent of the restoration method, and can be applied to any convolutional blur whose cepstrum is identifiable in spite of the presence of noise. The author's blur identification algorithm is described in Appendix C.

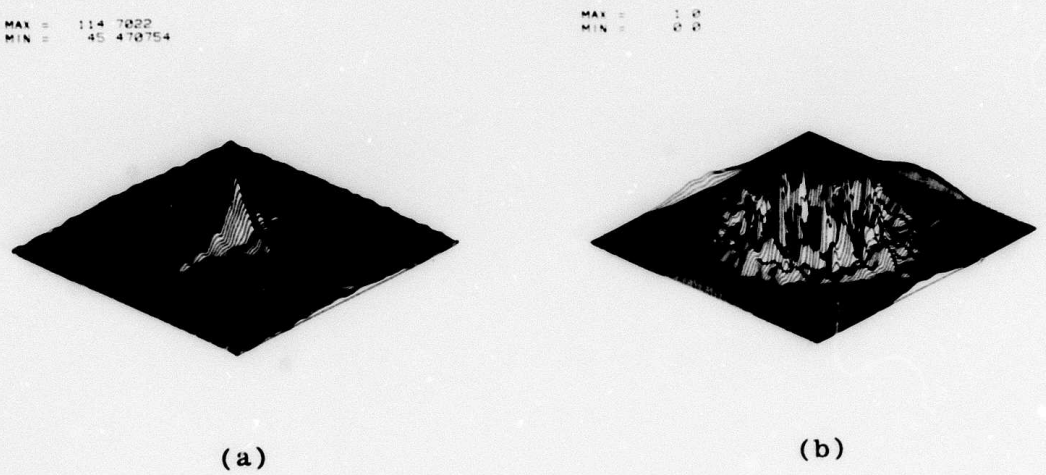

(a) (b)

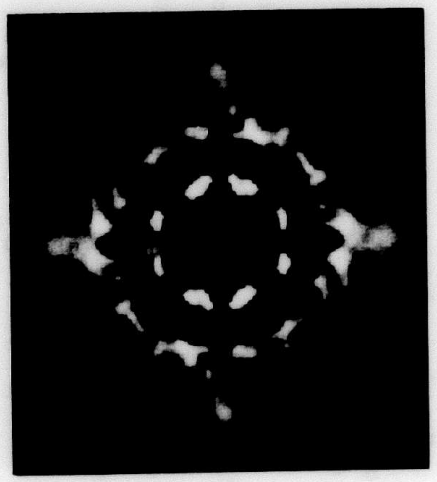

(c)

Figure 2.5

(a) The power spectrum of an out-of-focus image.
(b) The power cepstrum of the same image.
(c) An overhead view of the power cepstrum.

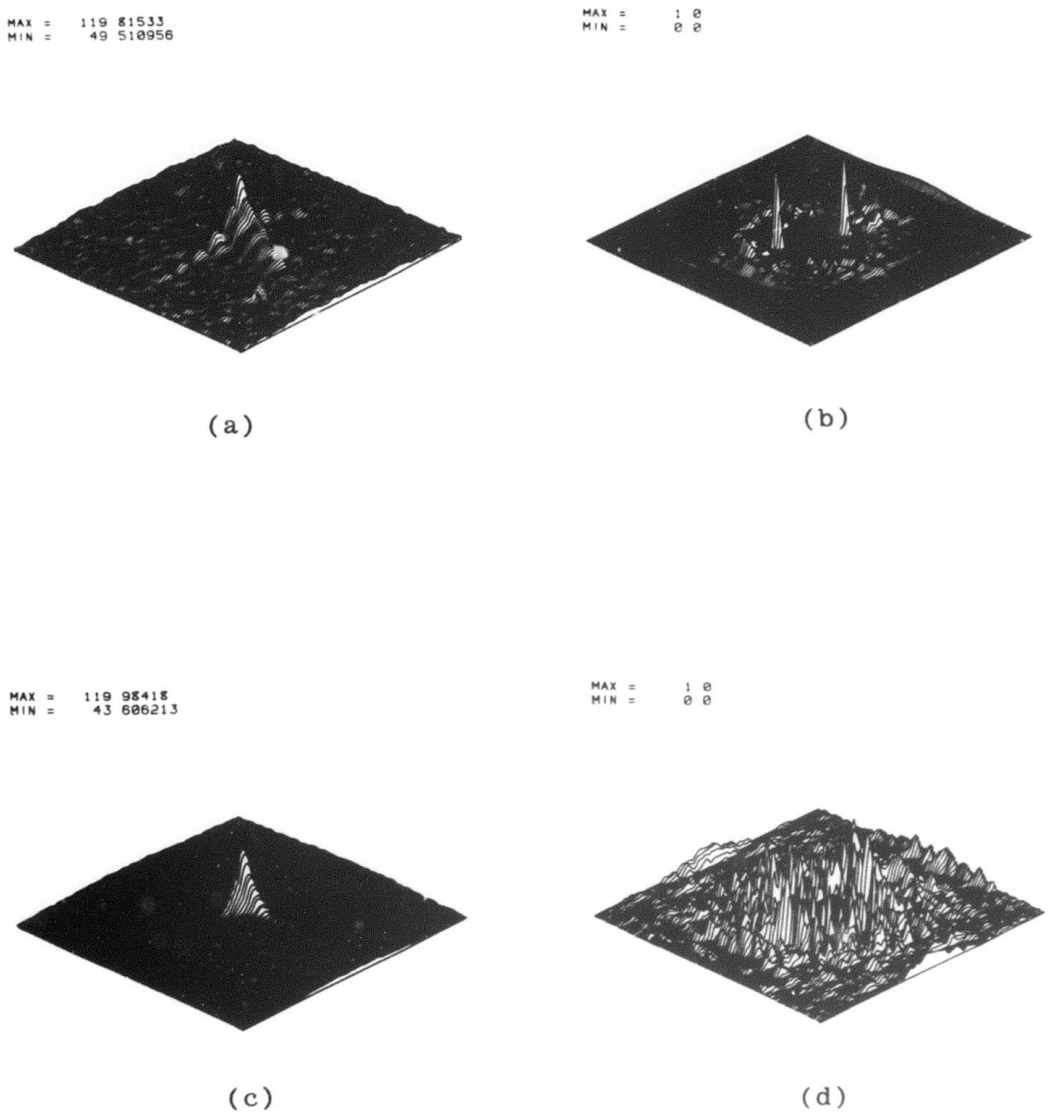

Figure 2.6

(a) and (b): The power spectrum and power cepstrum of a motion-blurred image.

(c) and (d): The power spectrum and power cepstrum of a turbulence-blurred image.

Combining now the phase of the blurf with the magnitude of the restoration filter of equation 2.3, we are in a position to attempt restoration.

2.5 Examples of Restoration by Power Spectrum Equalization

Figure 2.7 depicts the digital version of four blurred photographs. Figure 2.7a is a photograph of an eight story office building taken out-of-focus. Figure 2.7b (a photograph of a sign on a construction site) is also out-of-focus. Figure 2.7c is a motion-blurred photograph of the same sign. Figure 2.7d is a photograph of a sign blurred by atmospheric turbulence. This photograph was taken on a hot summer day through a telescope†† from a distance of two miles, thus resulting in an atmospheric turbulence blur.

Figure 2.8 shows the power spectrum of these four images, and Figure 2.9 the inverted and clipped power cepstra, under which the findings of the blur identification algorithm are listed. Figure 2.10 depicts $|H(f)|$ for each image. and Figure 2.11 the associated phase. Figure 2.12 shows the restoration kernels and finally, in Figure 2.13, the restorations of the four images are presented.

---

† In this particular case, it does not matter whether the phase or minus the phase is used, as one is equivalent to the other.

†† Field Model Questar, 2 second exposure on PAN-X.

The restoration of Figure 2.7a reveals the true relative width of the horizontal and vertical columns of the office building and discloses some previously indiscernable window panes. The small text on the Hilton signs is now decipherable. The echoes appearing in the Hilton restorations (and to a lesser degree in the others), are caused by the fact that the restoration kernels were windowed. The reason for windowing, as well as its effects, are discussed more fully in Chapter 5. The restoration of the sign in Figure 2.13d is interesting not because the blur was phaseless, but because noise dominates the restoration. The source of the noise can be readily explained if one examines the power spectrum of the blurred scene (Figure 2.8d) and the criterion for restoration. One will note from the power spectrum that noise dominates all higher frequencies. The criterion for restoration is that these noise-dominated frequencies will be amplified until there is as much power there as before blurring. In this case this power spectrum equalization criterion is too aggressive. This ill-conditioned situation could be avoided by re-sampling the data at a Nyquist rate which excludes these higher frequencies. An alternate solution is to change the method of restoration.

One of the features of the restoration system of Diagram 3 is that the restoration criterion can be changed. Chapter 3 presents several such criteria, including the criterion of least mean square error. It is well known that this criterion, which is not as

aggressive as the power spectrum equalization criterion, handles noise consistently well.

(a) (b)

(c) (d)

Figure 2.7
Four blurred digital images.

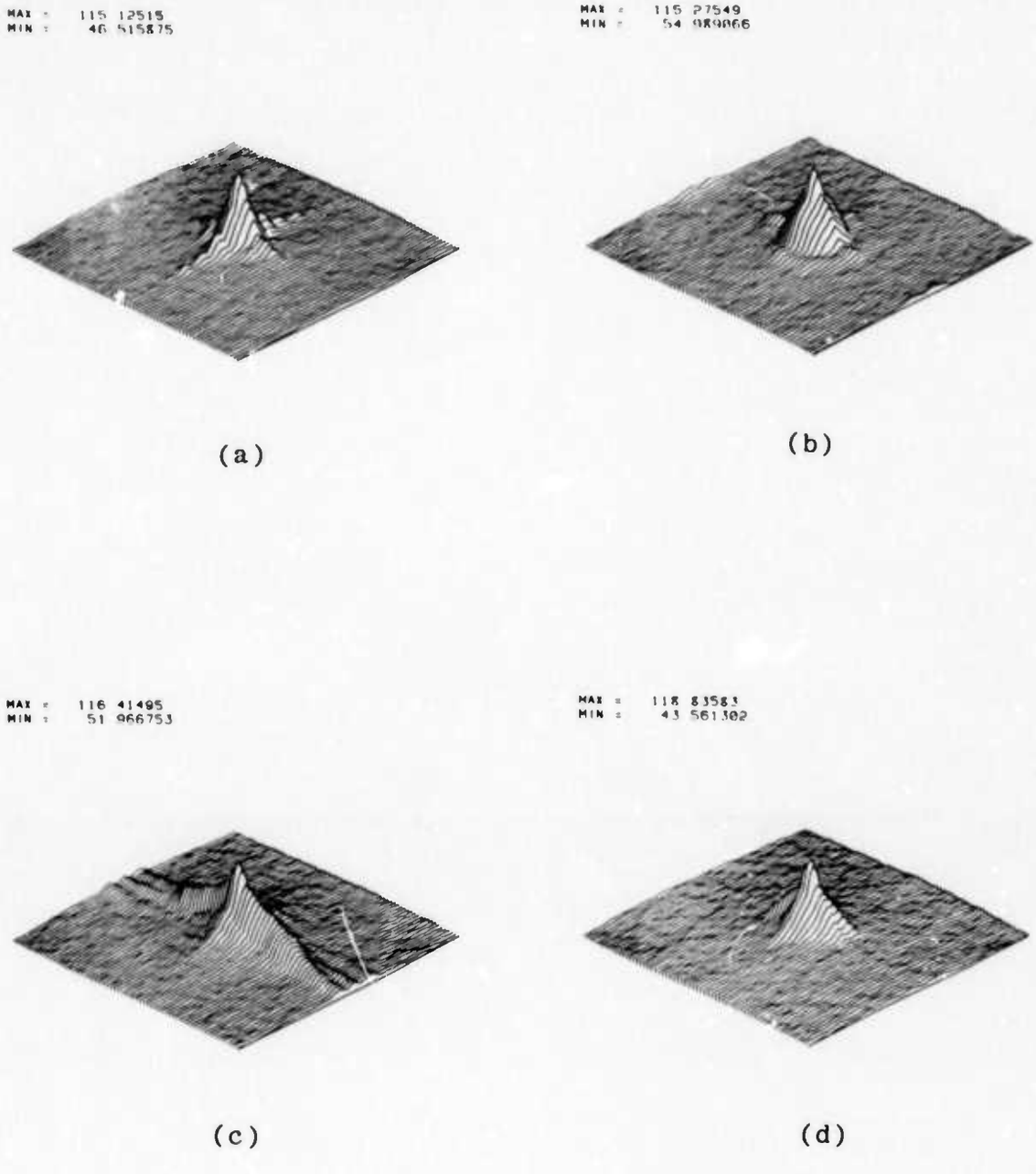

Figure 2.8
The power spectra of the images of Figure 2.7.

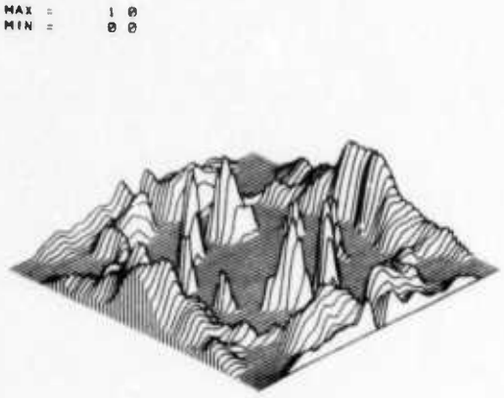

(a)
Out-of-focus blur
PSF of radius 7.8

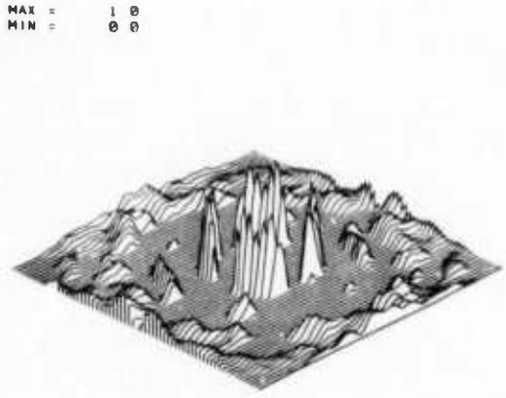

(b)
Out-of-focus blur
PSF of radius 4.5

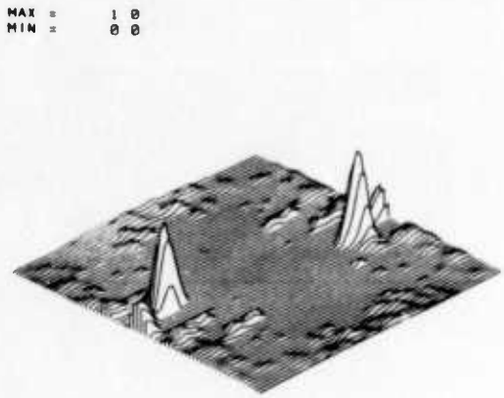

(c)
Motion blur
PSF of length 22, $\theta = 8.5^{o}$

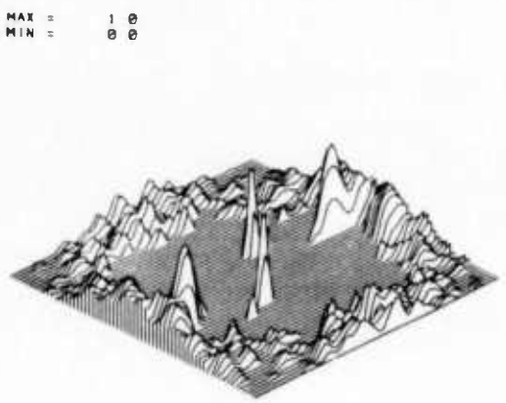

(d)
Turbulence blur

Figure 2.9

The power cepstra of the images of Figure 2.7. The findings of the blur-identification algorithm are listed under each cepstrum.

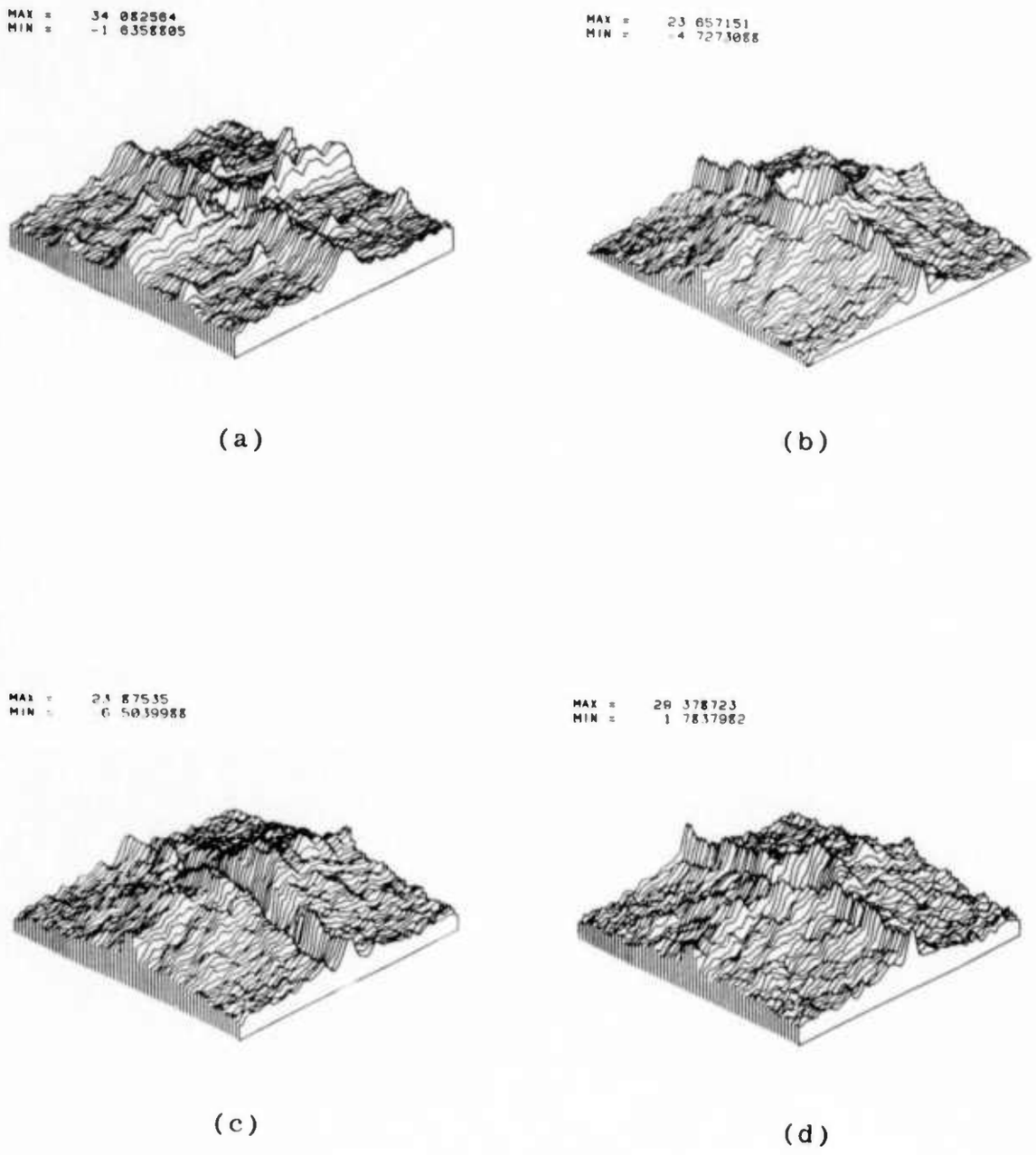

Figure 2.10

The magnitude of the restoration systems for the images of Figure 2.7

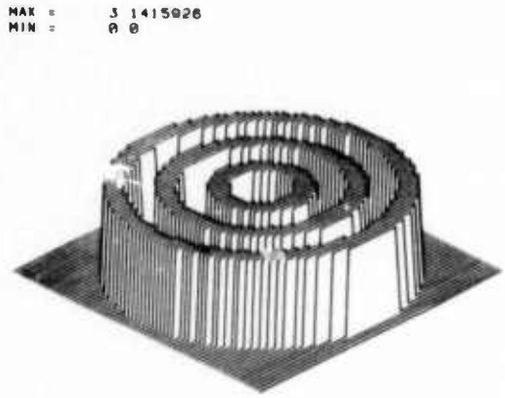

(a)

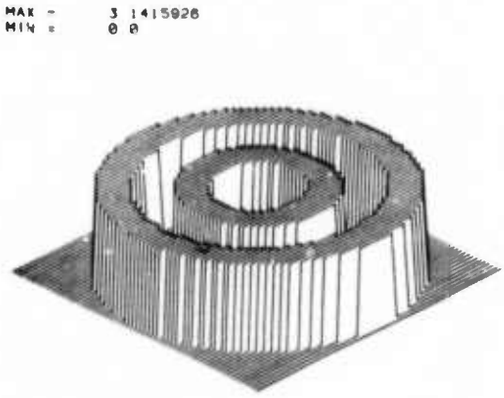

(b)

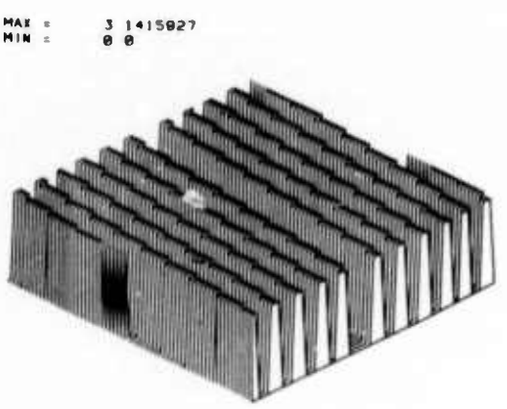

(c)

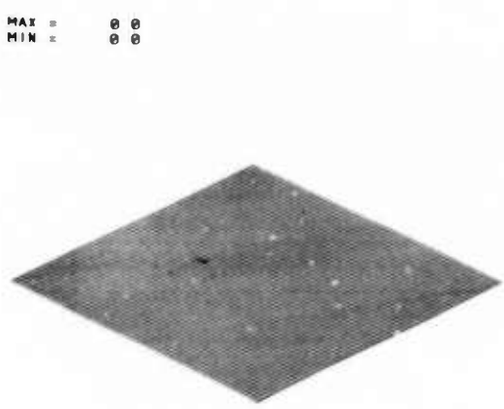

(d)

Figure 2.11

The phase of the restoration systems for the images of Figure 2.7.

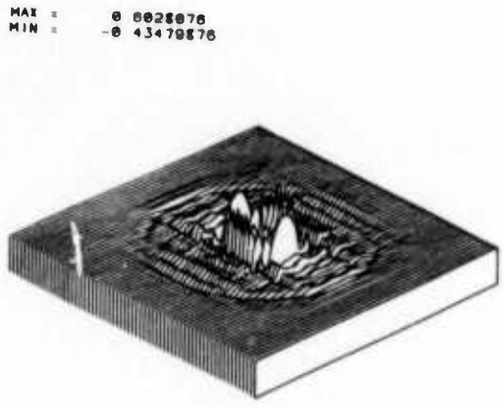

(a)

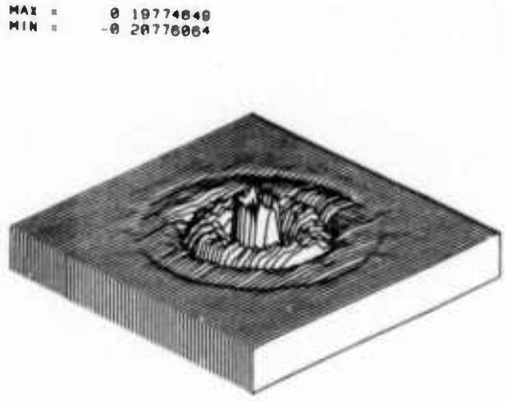

(b)

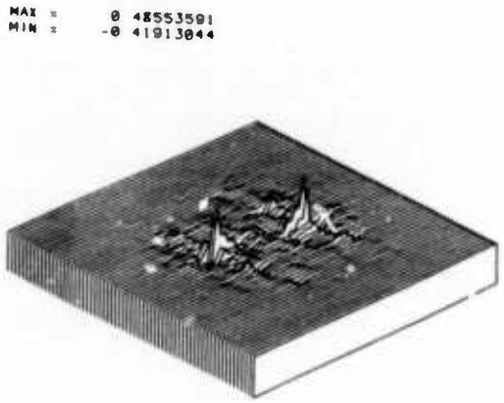

(c)

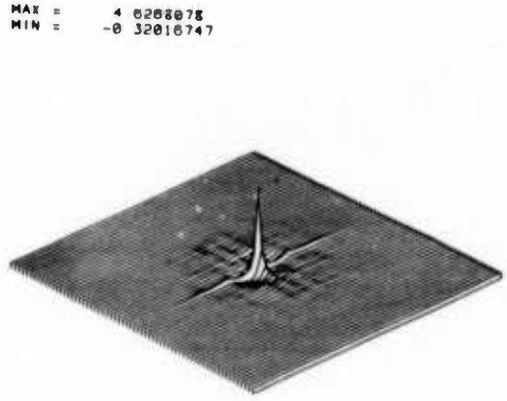

(d)

Figure 2.12
The restoration kernels for the images of Figure 2.7.

(a) (b)

(c) (d)

Figure 2.13

The restorations of the images of Figure 2.7. The restoration criterion was power spectrum equalization.

CHAPTER 3

Other Restoration Criteria

3.1 Minimization of Mean Square Error

A common criterion for restoration is that of minimizing the expected value of the square of the difference between the original image and the restored image. This concept is outlined in Diagram 4, where e is the quantity to be minimized.

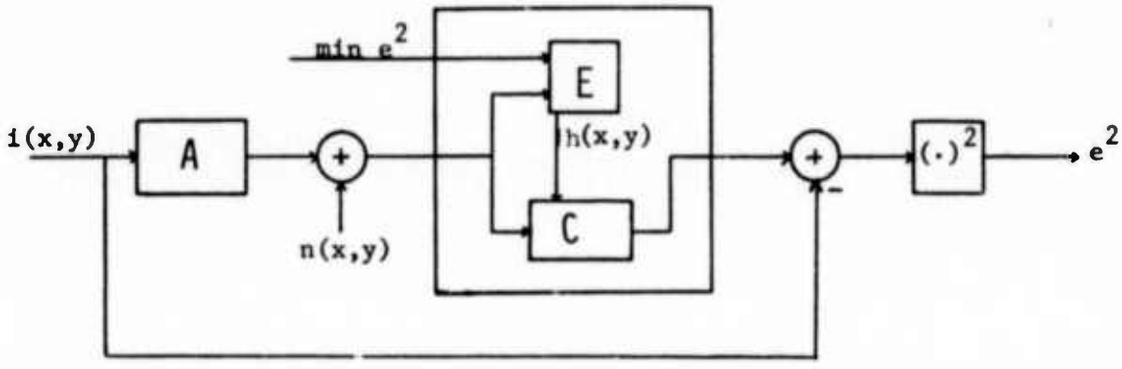

Diagram 4

The criterion of minimum mean square error constrains H to be:

$$H(f) = P_i(f)A^*(f)/[P_i(f)|A(f)|^2 + P_N(f)] \qquad (3.1)$$

The derivation of H(f) is given in Appendix D. The above restoration criterion and resulting restoration system strongly resemble certain aspects of Wiener filtering. The above system is fundamentally different, however, in that A(f) is not known a priori, but must be determined by the estimator, E, from each blurred input. The filter

can be computed by squaring the power spectrum equalization filter of equation 2.3 and multiplying by $A^*(f)$. The differences between the two filters, especially in terms of "aggresiveness", are elaborated upon by Cole.

In the case of motion blur and out-of-focus blur, $A^*(f)$ is readily determined from the blurred image itself via the power cepstrum. It was pointed out in section 2.4 that the spikes in the power cepstrum uniquely determine the nature and extent of the blur. From this knowledge one can compute $|A(f)|$ and $A^*(f)$, as well as the phase of $A(f)$. However, such information is not available in the case of turbulence blur. The necessary information can be obtained, though, from the power spectrum equalization filter of equation 2.3. It has already been pointed out that this filter approximates the inverse filter for those frequencies in which the noise power is small. For blurring resulting from turbulence, the filter assumes the form $-kx^2$ on a db scale, which is sufficient information from which to model $A^*(f)$ by curve fitting near the origin.

Figure 3.1 illustrates restorations of the blurred images shown in Figure 2.7 by the least mean square error criterion. The method of identifying the blur and computing the phase is the same as that discussed in section 2.4. The most significant change to be noted is in the restoration of the turbulence-blurred image in which the noise has been contained much more effectively. This example illustrates

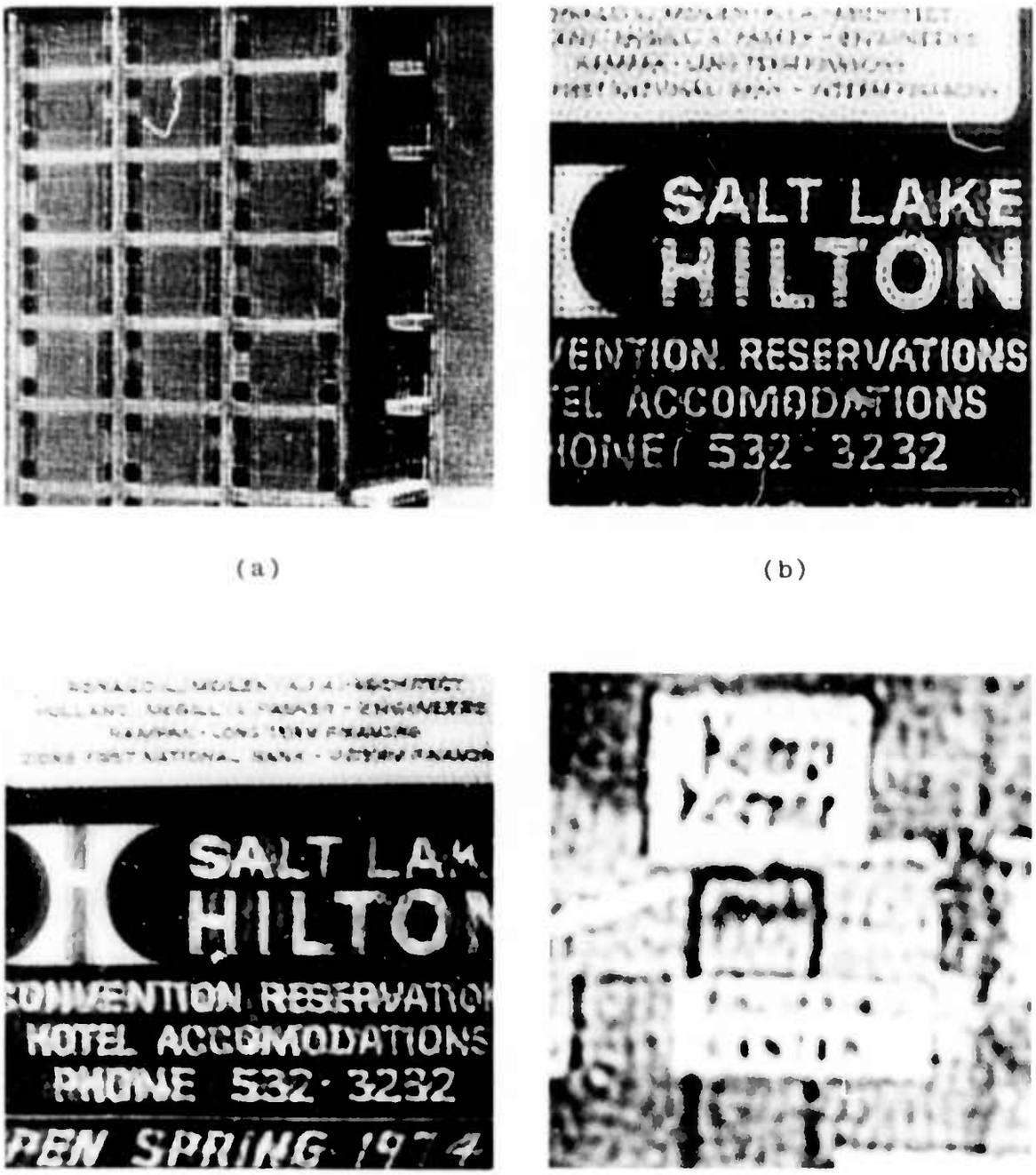

(a) (b)

(c) (d)

Figure 3.1

Restorations of the images in Figure 2.7 using the criterion of minimum mean square error.

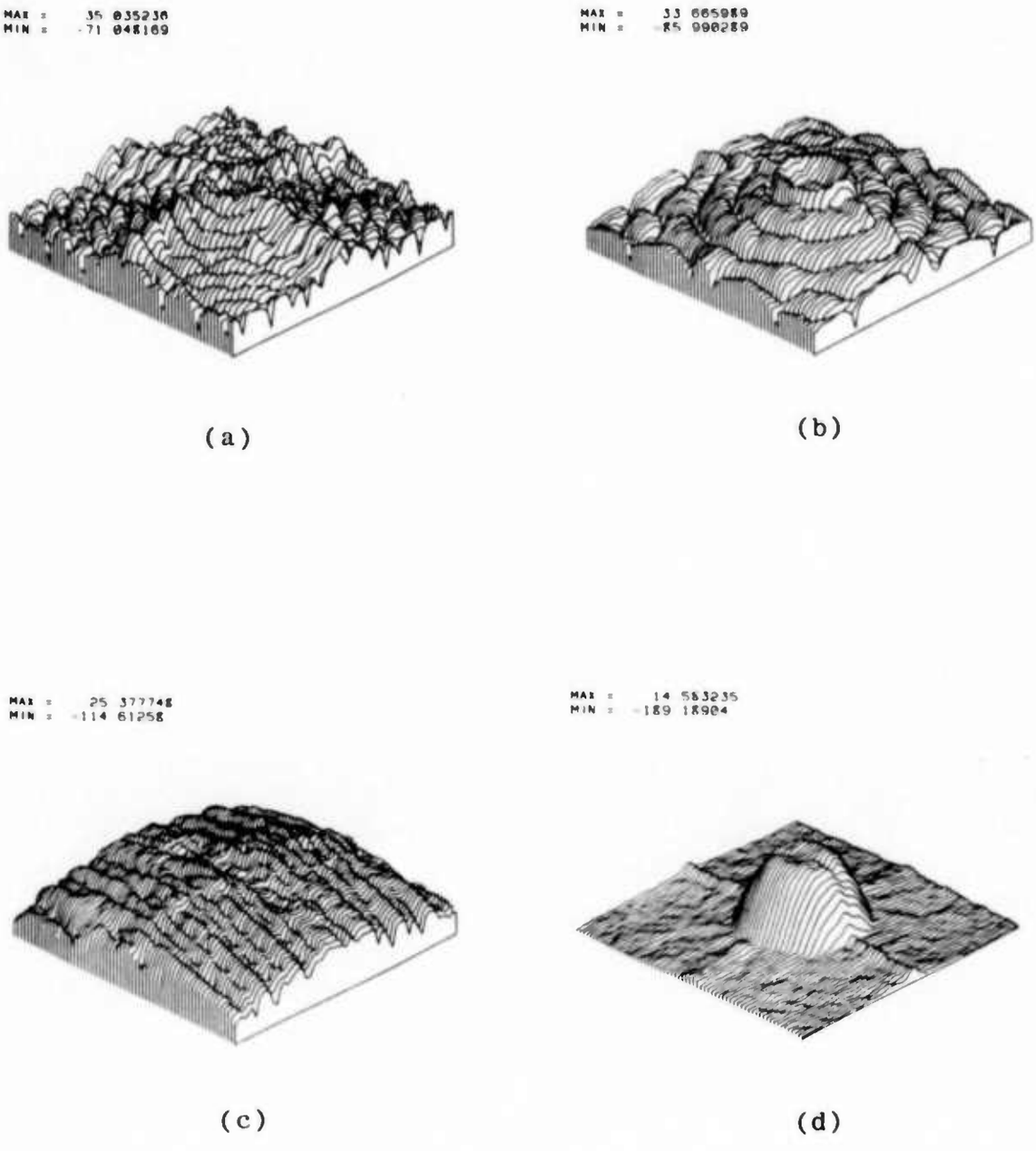

Figure 3.2

The magnitude of the restoration systems for the images of Figure 3.1. The magnitude of the turbulence system was not allowed to attenuate higher frequencies to the theoretical limit (-2000 db) as this would exceed the 36 bit capacity of the computer.

the fact that the minimum mean equare error filter is much less aggressive in the presence of noise than is the power spectrum equalization filter. However, this lack of aggresiveness is very evident in the poorer quality restoration of the fine text in the Hilton eigns.

3.2 Phaee-Only and Magnitude-Only Filters

Many inquiries have been made of the author concerning the effects of removing only the phase degradation or magnitude degradation in a blurred image. Such restorations of the motion-blurred Hilton eign are presented in Figure 3.3. These reetorations make evident the necessity of removing both the phase and magnitude componente of the blur. The phaee-only restoration is particularly interesting as it illustrates that the phase degradation of the blur, though necessary to remove, is small.

3.3 Inverse Power Spectrum Filter

The following reetoration criterion might be considered to be useful:

$$P_s(f)|H(f)|^2 = P_x(f) = 1 \tag{3.2}$$

Or:

$$|H(f)| = (1/P_s(f))^{1/2} \tag{3.3}$$

Thie criterion has produced fairly good results when used to remove

(a)

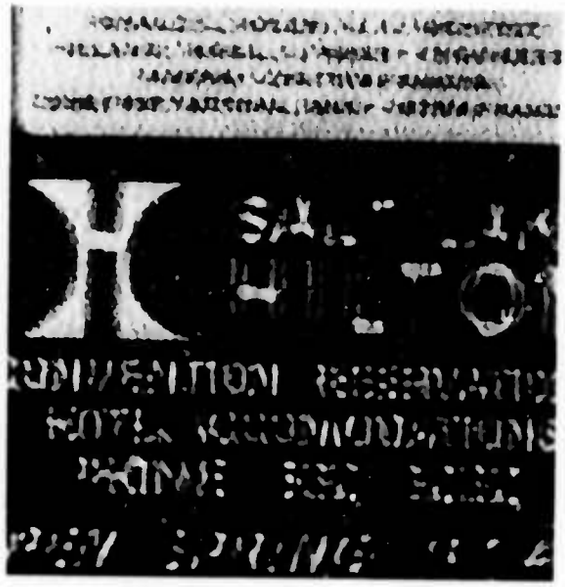

(b)

MAX = 0 23930292
MIN = -0 18737942

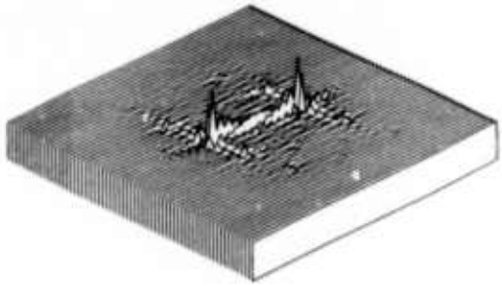

(c)

MAX = 1 685845
MIN = -0 1479092

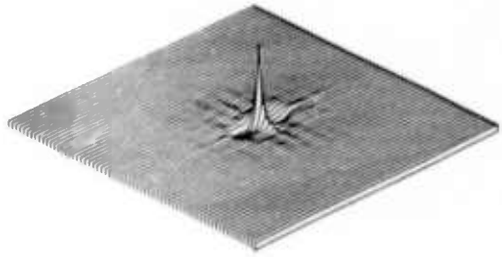

(d)

Figure 3.3

(a) A phase-only restoration of the motion-blurred Hilton sign.
(b) A magnitude-only restoration of the same sign. Under each image is shown the resulting restoration kernel.

narrow-band additive pollutants or reverberations from audio signals[12]. The criterion is inadequate, however, when applied to the present deblurring problem. This inadequacy results from the fact that the high frequency noise floor in the power spectrum of a blurred image is about 60 db† below the power of the lower frequencies. Inverting this spectrum and taking the square root results in boosting those noise-dominated frequencies by 30 db, which allows the noise to dominate the restoration. The power spectrum equalization filter boosts these frequencies by 5 db or less, and the minimum mean square error filter actually attenuates them.

3.4 Inverse and Hand-Tailored Inverse Filters

In light of the above discussion, the consequences of restoration by the pure inverse filter are readily predicted. Using the information contained in the power cepstrum of a blurred image, it is not difficult to determine the exact nature of the linear system that produced the blur and then to create its convolutional inverse. Restoring the office building with such a system results in the image shown in Figure 3.4a. This result supports the statement accompanying equation 1.9. Not only does the denominator of the inverse filter equal zero for certain frequencies, but this filter also boosts the power of frequencies that were dominated by noise after the blurring

---

† These numbers are empirical.

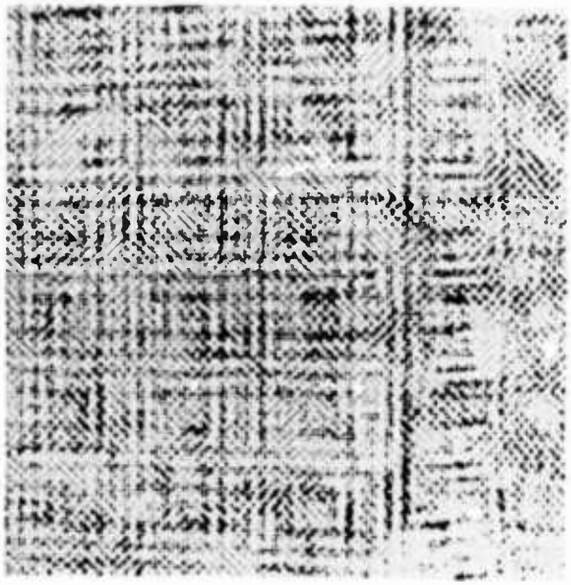

(a)

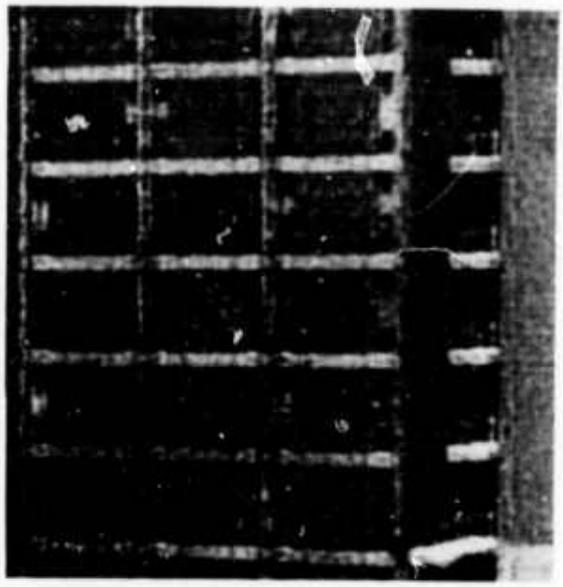

(b)

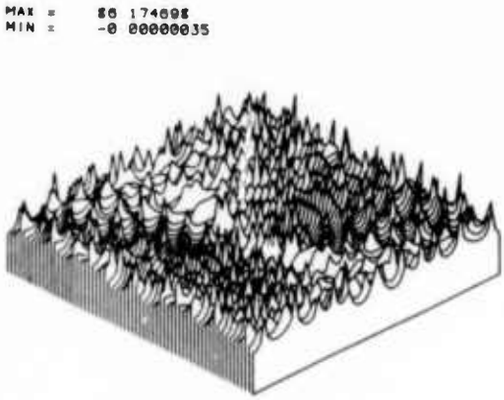

(c)

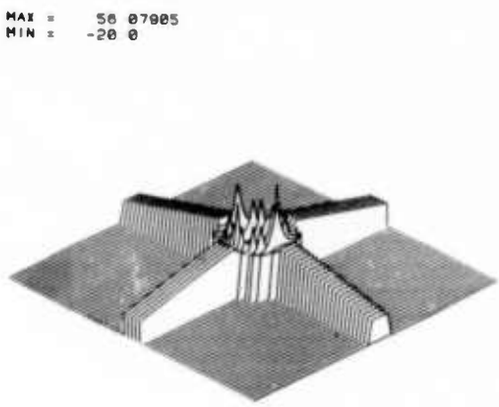

(d)

Figure 3.4

(a) The office building restored with a pure inverse filter.
(b) A restoration of the same image using a hand-tailored inverse filter.
The magnitude of the restoration systems are shown under each image.

occurred. The restoration of the blurred test pattern in Figure 3.5 illustrates that the latter of these two effects is by far the more serious degradation.

The restoration of 3.5d is the same as that of 3.5c with the exception that noise was added to the density version of the image before deblurring. One might correctly assume that containing the noise and restoring the image are two conflicting objectives. A common practice, however, is to suppress the gain in these noise-dominated frequencies, and then to clip the filter to eliminate zeroes in the inverse. The results of restoration with this hand-tailored inverse filter are shown in Figure 3.4b. This approach permits the design of a filter that will bring out specific information which might be overlooked by a more mathematically formal and rigorous filter.

These restorations demonstrate the fact that a knowledge of a(x,y) does not insure a meaningful restoration. Because of the ill-conditioned nature of the problem, great care must be exercized in the design of a successful restoration system.

3.5 Density Restoration

One of the notable flaws of the hand-tailored inverse restoration of Figure 3.4b, and of others previously presented in this work, is

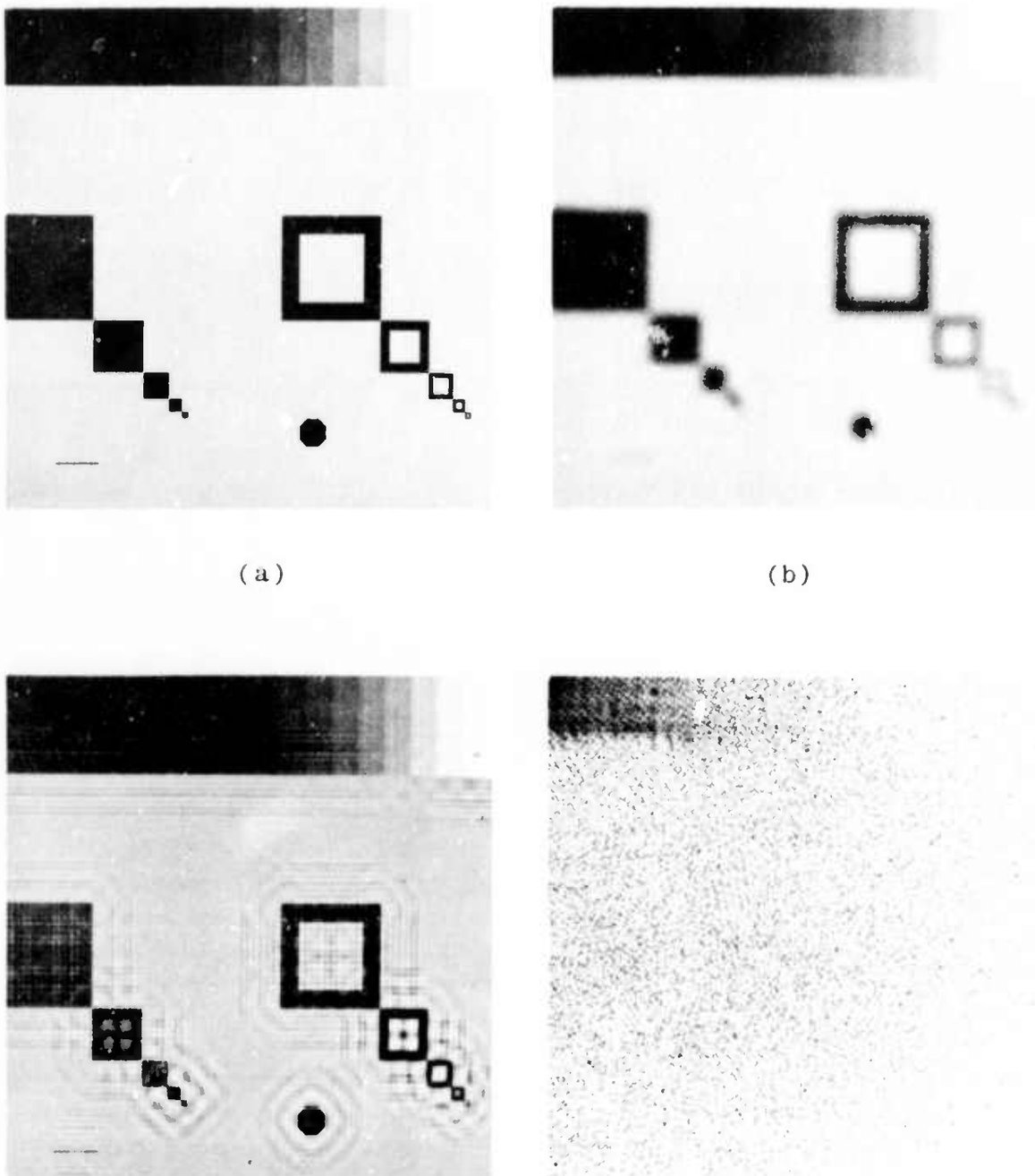

(a) (b)

(c) (d)

Figure 3.5

(a) A computer-generated test pattern.
(b) An out-of-focus version of the same pattern.
(c) A pure inverse restoration.
(d) A pure inverse restoration of a noisy version of the blurred pattern.

the presence of pure black areas in the restored image. These result from negative numbers in the processed image and are hence called "superblacks". Superblacks not only lack physical meaning, but are aesthetically unpleasant. Although the input to the restoration system is positive, there is no assurance of a positive output. In fact, work by Lukosz[13] and Boas and Kac[14] shows that the convolutional system that will guarantee a positive output (given a positive input) is opposite in nature to that of the restoration system which is needed for deblurring.

As a means of assuring a positive restoration, the author proposes restoring the density version of the image, as opposed to restoring the intensity version. Density† refers to the density of silver in the developed photographic image, and is proportional to the logarithm of the scene intensity which exposed the film. The last step in a density restoration is exponentiation, which insures the positiveness of the restoration. Two methods for accomplishing such a density restoration are now presented.

---

† For a complete discussion of the photographic density version of a scene, see "Fundamentals of Photography", by C. B. Neblette, Chapters 5 and 6.

3.5.1 Equalization of Density Power Spectra

Let us assume that the density version of the image was blurred, not the intensity version. The power spectrum equalization restoration criterion of equation 2.1 is then applied, where $P_s(f)$ and $P_i(f)$ are both estimated from densities. The results of performing such a restoration are shown in Figure 3.6. The phase information, however, must still be obtained as per Chapter 2, i.e., from intensity information.

3.5.2 Processing of Densities by the Intensity Restoration System

The restoration system, H(f), is generated from intensities according to the criterion of power spectrum equalization. Then, in lieu of restoring the intensity version of the blurred image, the density version is restored. In so doing, the logarithm is considered to be a linear scaling operation. Before deblurring, the image is scaled by 1/c (by taking the log), and after deblurring it is multiplied by c (by exponentiation). This procedure is most successful on scenes of low dynamic range. In this case the approximation is very good, i.e.,

$$\log(x+\delta) \propto c(x+\delta) \tag{3.4}$$

where δ is small.

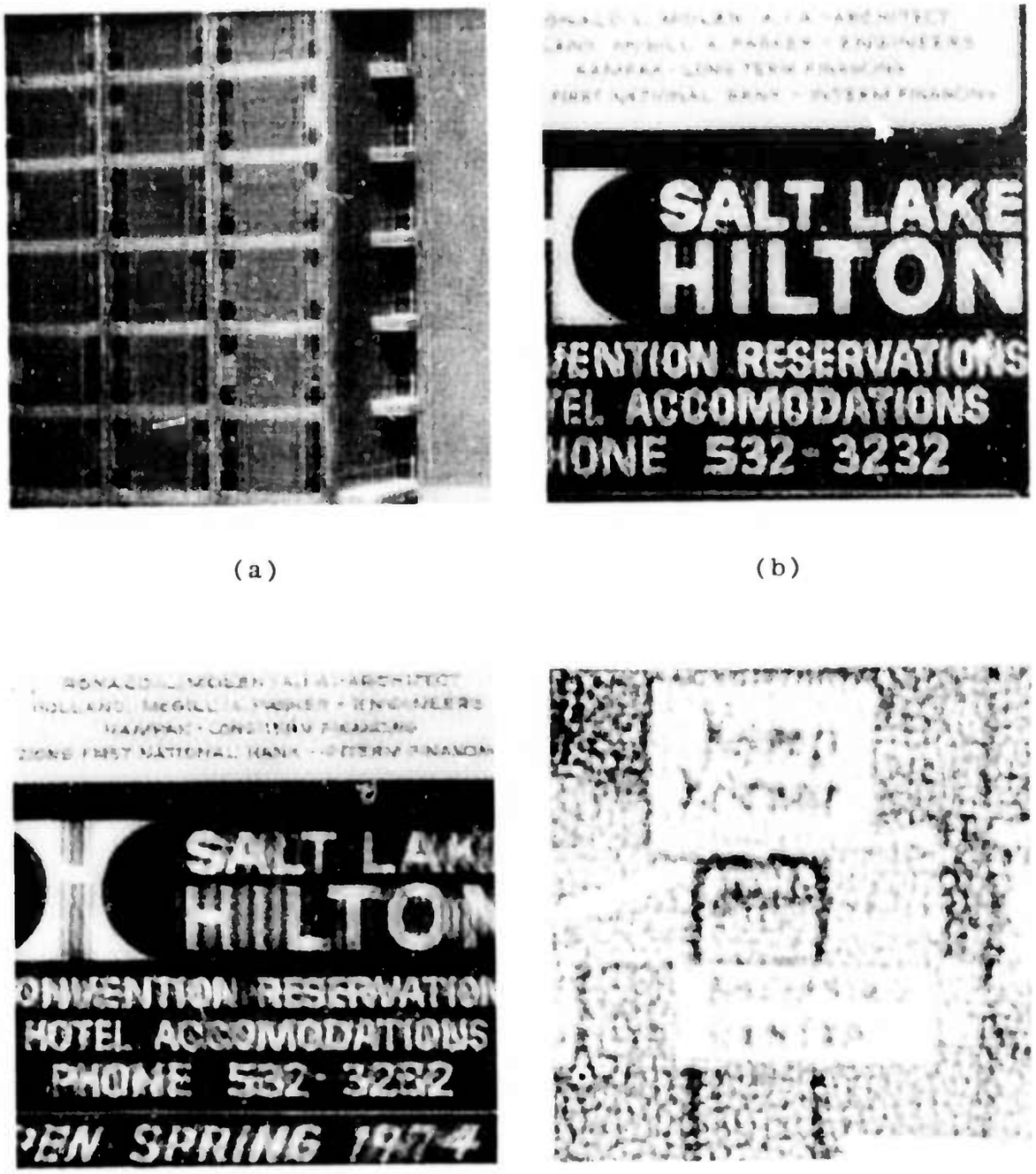

(a) (b)

(c) (d)

Figure 3.6

The blurred images of Figure 2.7 restored by the power spectrum equalization criterion applied to the density version of the images.

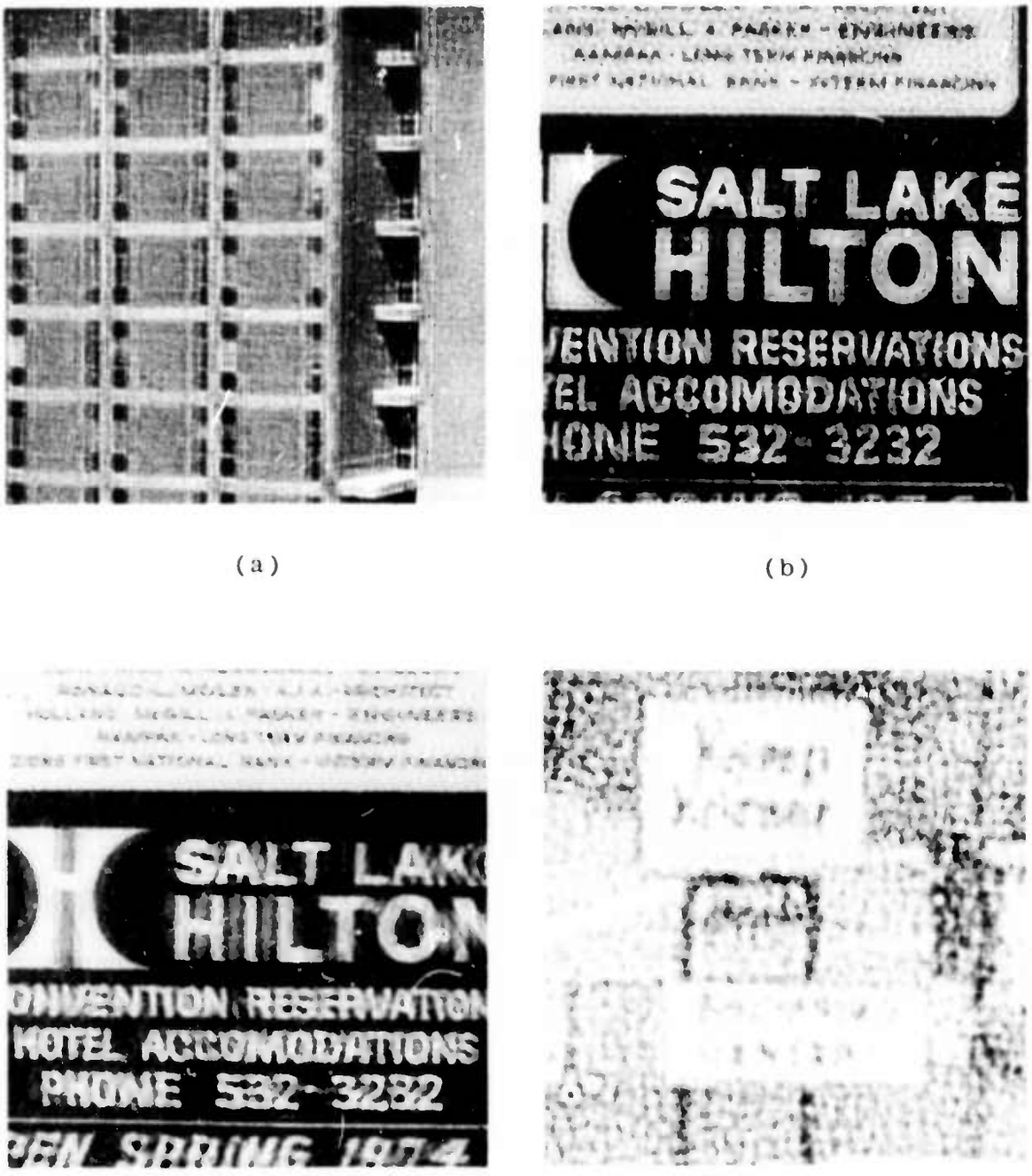

(a) (b)

(c) (d)

Figure 3.7

The blurred images of Figure 2.7 restored by passing the density version of the images through the intensity restoration filters of Chapter 2.

The results of this restoration procedure are shown in Figure 3.7. This procedure is basically different from the previous density restoration method, but in most cases the results are quite similar. The method is advantageous in that the power spectrum of the blurred image is also used for blur identification (i.e. to compute the power cepstrum) as well as for restoration.

In the case of a high dynamic range scene, the assumption that taking the logarithm can be viewed as a linear scaling operation may prove to be unsatisfactory. This is demonstrated in the restoration of the image shown in Figure 3.8a. The bright borders and dark echoes of the density restoration (Figure 3.8c) are artifacts of the nonlinearity of the logarithm. But even though such flaws are not evident in the intensity restoration, it is questionable if one restoration is actually superior to the other. The cause of the teardrop-like distortions in these restorations will be discussed in section 4.3.

3.5.3 Homomorphic Image Enhancment

The processing of the density version of an image not only insures a positive result but also allows for simultaneous image contrast enhancement as described by Stockham[15]. An intensity scene is composed of two components, the scene illumination and the object reflectivity, which are multiplied to yield the observed intensity.

(a)

(b) (c)

Figure 3.8

(a) A high-contrast blurred image.
(b) Intensity restoration by power spectrum equalization.
(c) Density restoration using the intensity restoration system.

Taking the logarithm of this scene transforms the multiplicative relationship into an additive one, as shown below:

$$i(x,y) = \text{illumination} \cdot \text{reflectance} \tag{3.5}$$

$$\text{Log}(i(x,y)) = \text{Log}(\text{illumination}) + \text{Log}(\text{reflectance}) \tag{3.6}$$

If the two quantities on the right of equation 3.6 occupy different frequency bands (and they do, roughly), linear filtering can be performed to enhance the term corresponding to the object reflectivity. The result of performing such a simultaneous deblurring/enhancement restoration of the office building is shown in Figure 3.9. The process produces a higher contrast image which is aesthetically more pleasing.

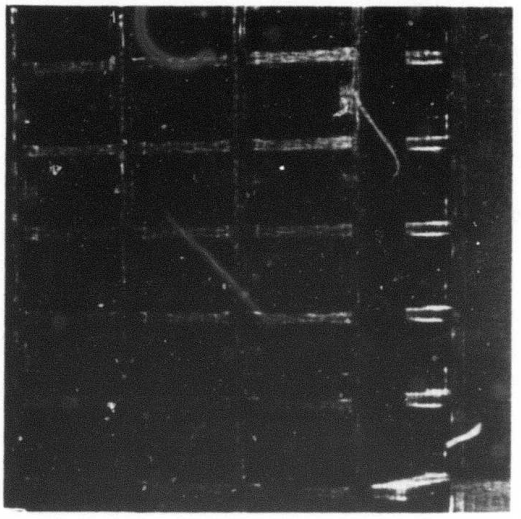

(a)

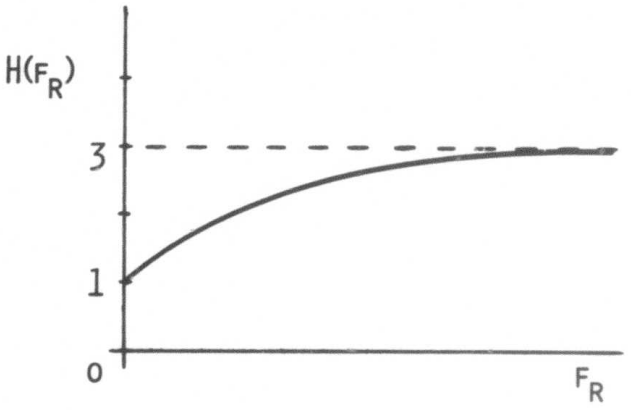

(b)

Figure 3.9

(a) A homomorphically-enhanced version of the restoration in Figure 3.7a.
(b) The frequency response of the enhancement filter.

CHAPTER 4

Effects of Noise

4.1 Sources of Noise

It was pointed out in section 1.2 that the blurred image itself is not available but rather a blurred image that has been contaminated by noise. Sources of noise may include sensor noise, transmission noise, scanner noise, and quantization noise. Noise may also be introduced by the storage medium, such as photographic film. Photographic film-grain noise is the greatest source of noise in the images considered in this thesis. Impulse noise is also of concern in this work. Impulse noise is caused by dust particles on the film or print used to store the image before digitization. The nature of these two sources of noise, namely film-grain noise and impulse noise, is discussed below.

4.2 Film-Grain Noise

Film-grain noise is caused by the tendency of the silver (halide) crystals in the photographic emulsion to clump together during development. The mean diameter of the crystals is on the order of 1 micron, and that of the clumps about 5 microns. This granular nature of the photographic representation of the scene is as though the

scene, as recorded on film, had been corrupted with random additive noise. But since this has been added to the logarithm of the scene (see footnote, section 3.5) the noise is really multiplicative, which Figure 4.1 illustrates quite graphically. The notion of preprocessing the logarithm of the data to reduce the effects of multiplicative noise has been explored by Cole[4].

The effects of film-grain noise are two-fold. As can be seen by examining the power spectrum of almost any blurred image, much of the higher frequency information contained in the image is dominated by the energy in the noise. Any attempt to retrieve this information by replacing the energy that blurring removed could result in the noise gaining so much energy that it would completely dominate the restoration. Such a case is shown in the inverse filter restorations of Figures 3.4a and 3.5d. Consequently, because of noise problems, the restoration system must be less aggresive, thus resulting in an imperfectly deblurred image. Much of the motivation behind the minimum square error filter and the power spectrum equalization filters is a desire to keep noise under control during restoration. In moderately noisy images both types of filters appear to perform equally well in containing the noise; the major difference between them being the amount of deblurring each accomplishes.

A second effect of noise is an advantageous one. In the denominator of many of the restoration filters described herein there

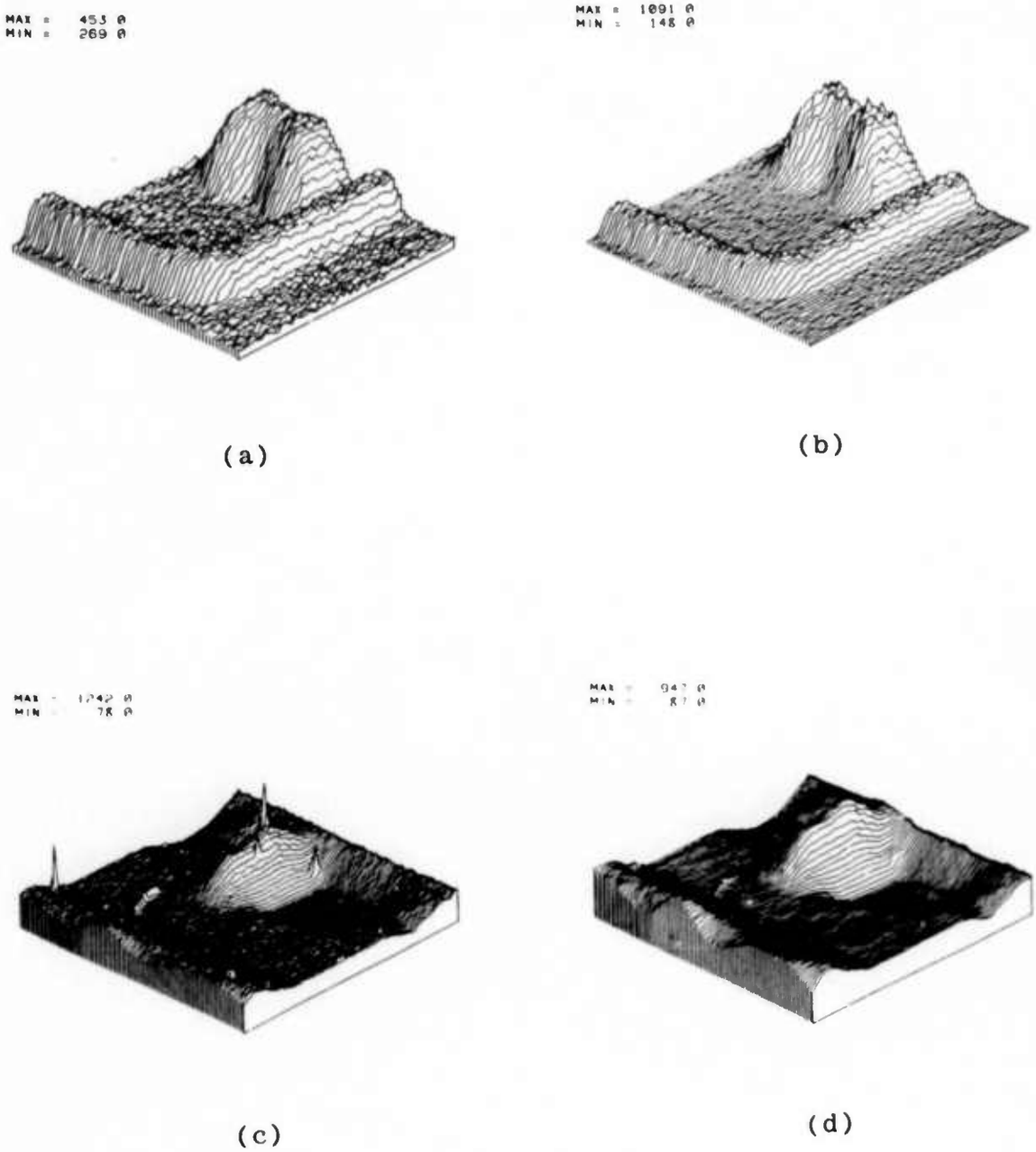

Figure 4.1

(a) A section of the density version of a (blurred) image.
(b) A section of the intensity version of the same image.
(c) A section of the office building image.
(d) The same section after Tuckey filtering.

occurs the term $P_s(f)|A(f)|^2 + P_n(f)$. In the case of motion blur and out-of-focus blur, A(f) equals zero for certain values of f. The zeroes are particularly troublesome in that they occur at the same frequencies as the zeroes of the blurring system. These frequencies have been contaminated by noise, and division by A(f) would result in infinite amplification of these noise-dominated frequencies. However, the addition of the power in the noise to the denominator of the restoration filter moderates this intrinsically ill-conditioned situation.

It is difficult to constrain a filter to handle film noise in a mathematically precise manner. The minimum square error criterion comes close to doing so in the present deblurring problem, but only after two assumptions are made. The first is that the noise is added to and uncorrelated with the signal; the second is that the statistics of the signal are stationary (see Appendix D). Figure 4.1b shows the first assumption to be incorrect, and a glance at any common photograph places the second assumption in question. However, the deficiencies of these two assumptions may be self-canceling in that the noise varies with the signal. The ratio of the two, which is found in many restoration filters, remains approximately constant, thus allowing the filter to perform as though these assumptions were indeed valid.

4.3 Impulse Noise

A second type of noise, which is quite different from film-grain noise, is impulse noise. Impulse noise is caused by small specks dust on the film during exposure (resulting in an unexposed spot on the film) or on the film during scan-in (resulting in a pure white spot in the image). The effects of this noise are most visible in the restored images of Figure 3.8. Small specks of dust, which are barely discernable in the original image, have assumed Gargantuan proportions in the restoration. This is the result of the restoration kernel being convolved with a large impulse, the result of which is the kernel itself.

Most of the images in this thesis were either edited "by hand" to remove these spikes or were subjected to a more sophisticated scheme such as the resistive filter proposed by Tukey[16]. The Tukey scheme is nonlinear and consists simply of setting the value of each point equal to the median value of its neighbors. The process obeys scalability but not superposition over addition. That is, a constant times the input yields the same constant times the original output, but input one plus input two does not equal output one plus output two. Applying the Tukey filter to any monotonic function of the data results in an output operated on by that same function. It therefore makes no difference whether the density version or intensity version of the image is filtered. The result of having "Tukey-filtered" a

section of the office building is shown in Figure 4.1d.

The Tukey filtering procedure is well suited to the removal of noise spikes from blurred data. The filter tends to remove abruptly changing features of the image while leaving gently varying data relatively untouched - blurred data is gently varying, the noise spikes are not. The procedure is also pleasing from an energy point of view. Were the image low-pass filtered to remove the noise spikes, much of the energy associated with these spikes would remain in the image. The Tukey scheme, on the other hand, removes the spikes and the energy associated with them almost entirely.

4.4 Noise and the Reflection Scanner

Most of the images in this thesis were not digitized directly from the film itself, but instead from a print of the film scanned on a reflection scanner. One might suppose that this would compound the film-grain noise in that the graininess of the print would be included in the scanned-in image. To investigate the effect of this additional grain noise, several images were digitized directly on a scanning microdensitometer†. The power spectra of these images were compared with the spectra of the same images that had been scanned on a

---

† Drs. B. R. Hunt and D. H. Janney of the Los Alamos Scientific Laboratory offered their time and facilities to do the actual scanning of the images. The out-of-focus Hilton sign is one such image.

reflection ecanner. Such a comparieon is shown in Figure 4.2.

Close inepection of the two power spectra reveals that the noise floor has not been altered at all. In fact, any variatione between the two can probably be ascribed to differences in the shape of the scanning aperture of the two input devices. The Utah aperture is gaueeian in ehape, the other ie rectangular, and both were set to measure approximately a 100 micron spot. The reason for the film-grain noise not being increased by the reflection scanner process ie that the printing paper is much slower than ordinary film, and hence much less grainy. Therefore, the graininess seen by a reflection ecanner is that of the film, not the print.

If printe are made avoiding the toe and shoulder regions of tne D log E curve of the paper (and are compensated for this after scanning), results can be obtained that are nominally equal in quality to that of a scanning microdensitometer. This applies, of course, to the present application only - there are many instances in which extremely wide dynamic range and the need to investigate actual film-grain structure (as well as ease of operation) necessitate the use of euch an instrument.

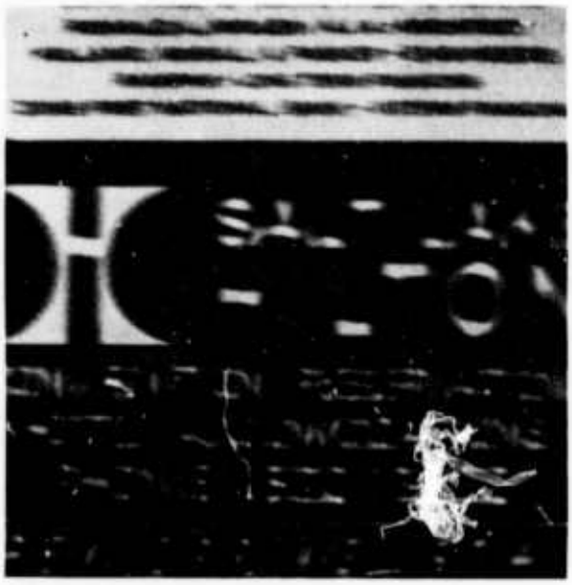

(a)

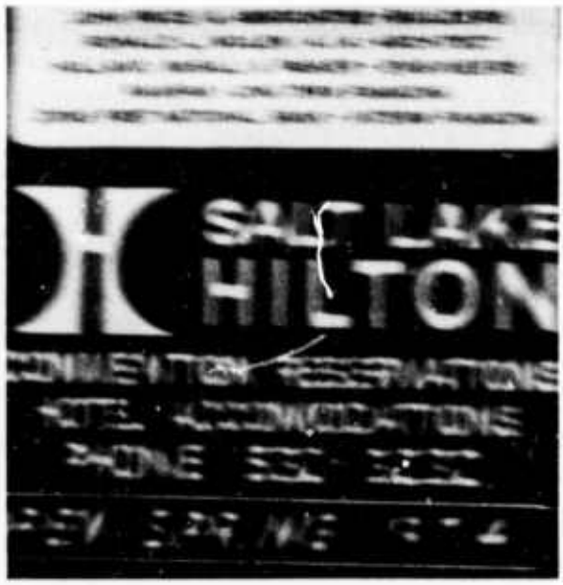

(b)

MAX = 116 41495
MIN = 51 966753

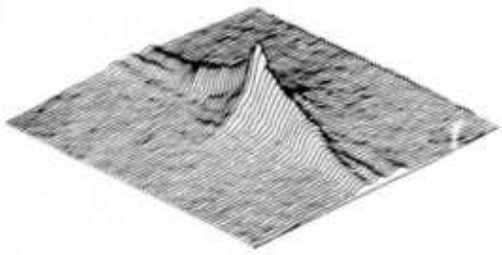

(c)

MAX = 115 91731
MIN = 53 774216

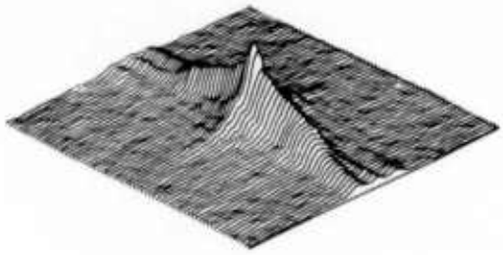

(d)

Figure 4.2

The Hilton sign scanned on (a) a reflection scanner and (b) a scanning microdensitometer. Below each is the respective power spectrum.

CHAPTER 5

Conclusion

5.1 Review of Restoration Method

The goal of this research is to restore a blurred image using a minimum of knowledge about the particular image or blur involved. The nonlinear homomorphic restoration system of Chapter 2 (Diagram 3) was presented as a solution to this problem for the case in which the blur (1) can be modeled as a linear system and (2) has a uniquely identifiable cepstrum. The success of this solution has been demonstrated using three distinct types of such blurs.

Several restoration criteria have been presented including power spectrum equalization, minimum mean square error, as well as the hand-tailored inverse restoration. Results indicate that the preferred restoration procedure, in terms of aggresiveness vs noise handling capabilities, is the processing of densities with an intensity restoration system that was estimated in accordance with the power spectrum equalization criterion. This procedure is not only sufficiently aggresive, but also insures a positive result and allows for simultaneous contrast enhancement. Although this procedure may fail in the case of a severe blur in which noise dominates most higher frequencies, such cases are readily handled by the minimum mean square

error criterion.

5.2 Remaining Problems

The homomorphic restoration method presented in Chapter 2 is only successful on a limited set of blurs, and is by no means a solution to the general deblurring problem. Some remaining problems, and a few suggested solutions, are presented below.

5.2.1 Ringing

One of the obvious flaws in the restorations presented in this thesis is the presence of ghost-like echoes, or ringing, in the deblurred image. This phenomenon results from the fact that h(x,y), the restoration kernel, is not allowed to extend to infinity, as it theoretically should. If the convolution is to take place in a reasonable amount of time, the kernel must be truncated to be, say, 64 points wide by 64 points long. It is then windowed with a Hanning window. The restoration kernel performs the deblurring (roughly speaking) by adding and subtracting shifted copies of the blurred image. Tampering with this kernel hinders it in doing a perfect job, and results in remnants of these shifted copies remaining in the restored image. Figure 5.1 illustrates this effect on a test pattern. The restoration shown in Figure 5.1a was performed with a 128x128 restoration kernel and the restoration in 5.1b with a 64x64 kernel.

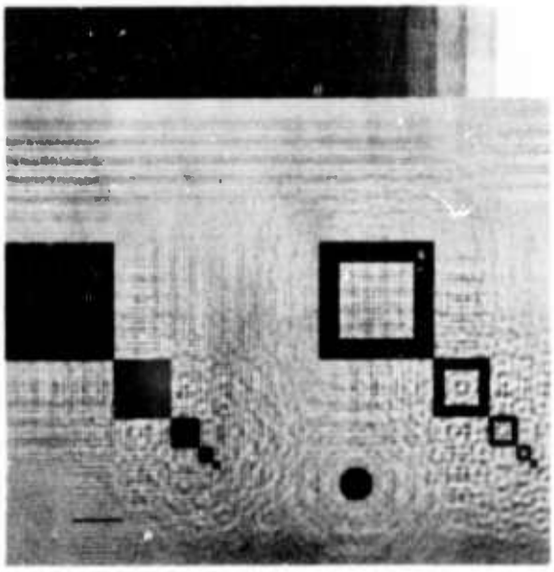

(a)

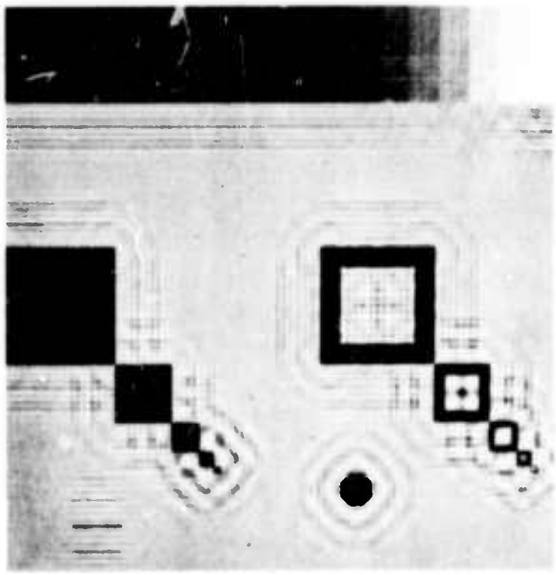

(b)

Figure 5.1

Two restorations of the blurred test pattern of Figure 3.5b using (a) a 128x128 kernel and (b) a 64x64 kernel.

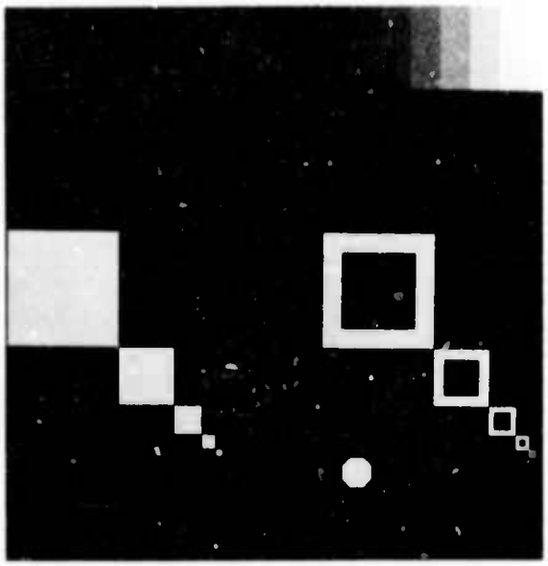

(a)

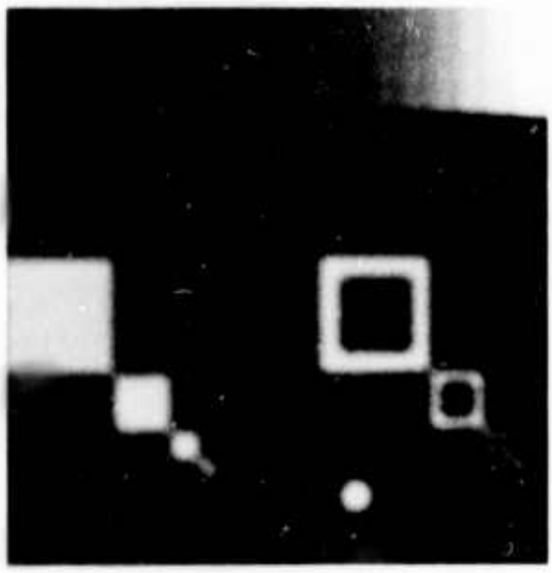

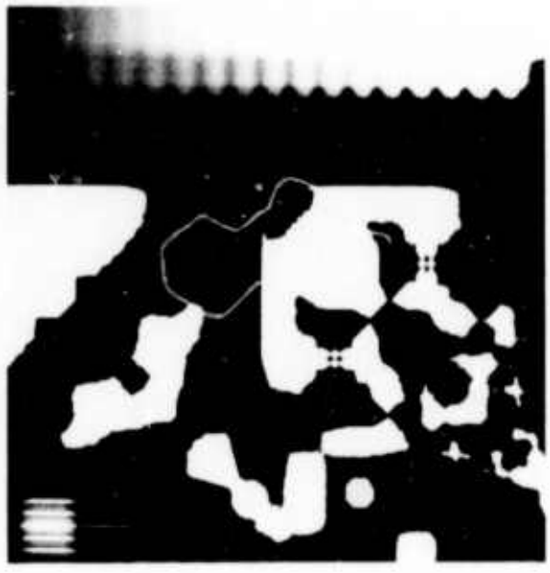

(b) (c)

Figure 5.2

(a) A computer-generated test pattern.
(b) A blurred version of the pattern.
(c) A restoration using an unwindowed kernel. Note that the octagon and the line were successfully deblurred.

Although the ringing in the former restoration covers a larger area, it is much less pronounced. It would indeed prove advantageous from a computational point of view to achieve the results of the larger kernel using only a modified version of the smaller kernel. The strategy for making such a modification is yet to be devised.

The ringing not only surrounds each object but is superimposed upon the objects themselves. Thus, the more variety present in an image, the more severe are the effects of ringing. Conversely, the less variety, the less severe are these effects; an important class of images is included in this latter case. Consider an object photographed against a dark background, such as a satellite against the background of space. A restoration with an unwindowed kernel might prove optimal. Such a kernel would restore perfectly in the area of the object, and very poorly elsewhere. This case is illustrated in the restoration of the slightly modified test pattern shown in Figure 5.2.

5.2.2 The Space-Variant Blur

It has been assumed in this thesis that the blur is constant over the entire image. The problem becomes very difficult[10] if the blur changes in severity in different regions of the scene. The present method may show promise, however, if the blur changes gradually over the image. In this case, the image could be divided into sections;

the average amount of blur could then be estimated in each section. For example, if a motion blur progressed in severity from left to right, one might divide the picture into halves and treat the problem in two parts.

If the image had to be divided into many sections, the method of phase estimation by the cepstral technique would begin to fail, as an average over at least 20 picture subsections is required. In this case, the zero crossing technique would prove valuable, as it produces reliable results after averaging over as few as two (possibly overlapping) subsections.

5.2.3 A Mixture of Blurs

Thus far we have assumed that a particular image had been blurred by only one type of blur, i.e., motion blur, out-of-focus blur, or turbulence blur. The system for restoring such images is completely automatic; the same system can also be applied to a combination of blurs, but then automation becomes difficult. Figure 5.3a illustrates such a case. The lens was not only defocused when the scene was photographed, but the camera was also in motion.

Figure 5.3d shows the inverted and clipped power cepstrum of the scene. Characteristic spikes of both motion blur and out-of-focus blur are plainly visible, which is to be expected from a theoretical

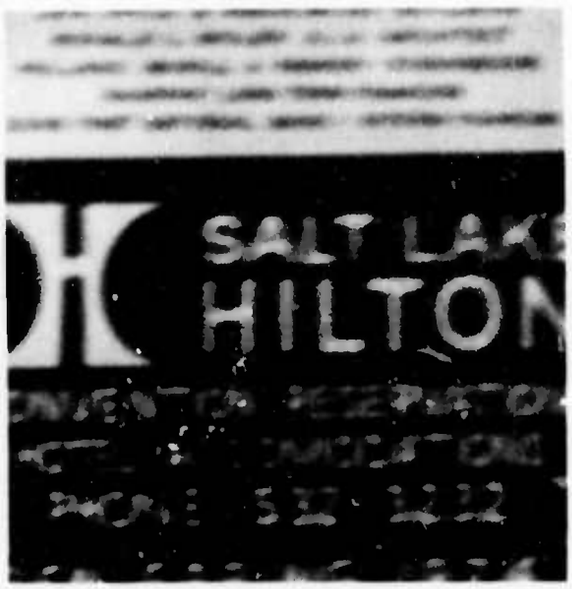

(a)

(b)

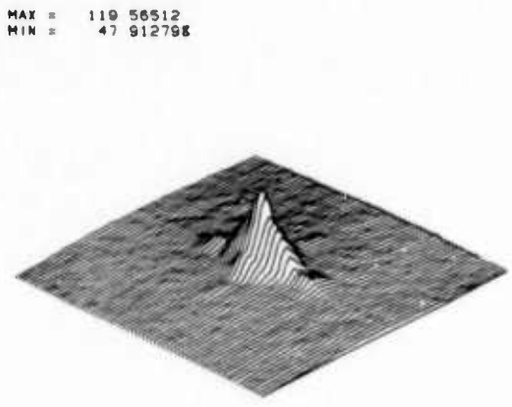

(c)

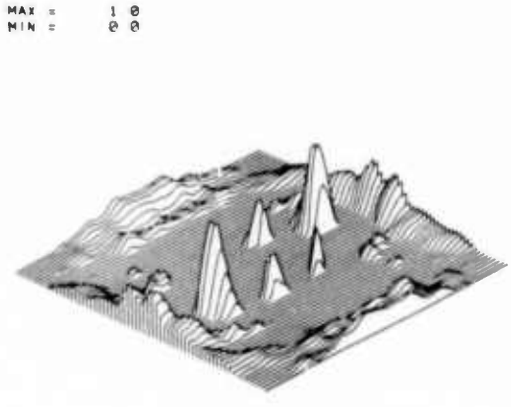

(d)

Figure 5.3

(a) An image that was blurred by a moving out-of-focus camera.
(b) The restoration of that image.
(c) The power spectrum of the blurred scene.
(d) The power cepstrum of the blurred scene.

point of view. The blurred image consists of the original scene intensities that have been passed through two linear systems, i.e.,

$$b(x,y) = i(x,y) \circledast a(x,y) \circledast d(x,y) \tag{5.1}$$

Computing the cepstrum in a manner analogous to that of section 2.4 yields:

$$C_b(q) = C_i(q) + C_A(q) + C_D(q) \tag{5.2}$$

where $C_A(q)$ and $C_D(q)$ are the cepstra of the two blurs, and are simply added together in the cepstrum of the blurred image. It is not difficult to distinguish visibly between these two cepstra and to generate the phase associated with each. This procedure has been followed to produce the restoration shown in Figure 5.3b. The data in the power cepstrum was examined to locate the position of the twin peaks of motion blur and to determine the radius of the ring of spikes resulting from out-of-focus blur. However, an automatic algorithm for handling a mixture of blurs has not yet been devised.

5.2.4 Automatic Prototype Selection

It was explained in section 2.2 that the power spectrum of the clear image, $P_i(f)$, was estimated from a scene considered to be statistically similar to the blurred image under consideration. The selection of the similar scene is a manual one, and is the only portion of the restoration process (of a single blur) which is not automated. Although many methods might be proposed to determine the

statistical nature of a scene from a blurred version of it, work by Rom[8] shows special promise. Rom has shown that the cepstrum of an image contains an abundance of information concerning the statistical nature of the image itself. Adapting these results to an approach using the power cepstrum may prove to be successful.

5.3 Summary

The homomorphic restoration system presented in this thesis is not successful in restoring all classes of blurred images. The blurs that can be successfully treated, however, include a large subset of those encountered in modern imaging systems. The nonlinear restoration system is not only versatile and flexible, but also enjoys the solid foundation of standard linear system theory. The method of restoring these blurs is particularly advantageous in that it lends itself readily to automation. In addition, the process consumes only a modest amount of computation time, insures a positive definite result, and allows for simultaneous contrast enhancement.

APPENDIX A

Power Spectrum Estimation

The method used in this work for the estimation of the power spectrum of an image is that set forth by Welch[9]. When applied in two dimensions, the method consists of subdividing the image into K equal and possibly overlapping square sections of width L. The sections are then windowed (by a Hanning or Parzen window) and Fourier transformed. The power spectrum is then estimated by computing the average of the square of the magnitude of these transforms. The method assumes that the ensemble of images under consideration is ergodic.

There are several variations possible, depending on the type of information needed from the power spectrum. Increasing the size of L results in increased resolution in the power spectrum, as more points are then used to cover the same band of frequencies. Increasing the size of K increases the degree of convergence of the spectrum. If a finer frequency grid is desired without loss of convergence, one augments each LxL section with zeroes after windowing.

It has been found that an average over 50 64x64 sections contains sufficient information for a successful restoration. If more

resolution is required, say for the zero crossing technique of phase estimation, a 128x128 estimation is adequate. Figure A-1 shows, however, that averaging only two sections results in an acceptable restoration; this saves considerable computation time, as pointed out in Appendix B. Figure A-2 shows the result of doubling the resolution of the power spectrum of a motion-blurred image, thus revealing clearly the lobes of the sin(x)/x component.

The astute reader will no doubt have noticed that the author has made use of the power spectrum to describe and determine the nature of the blurring system, whereas others[4.6] have computed a quantity called the average log spectrum. This is computed in the same manner as the power spectrum except that the average is over the logarithm of the magnitude squared of the transform of the picture subsections. Taking the logarithm is theoretically pleasing in that each subsection represents a mapping from convolution into addition. In practice, however, the approach has some drawbacks. Figure A-3 compares the result of computing the average log spectrum vs taking the log of the power spectrum. It is easily seen that the power spectrum contains more information pertaining to the slanted roof of the portico than the average log spectrum. Therefore, the use of power spectra allows the relationship of Eq. 2.1 to convey more information than if the average log spectrum were used. The theoretical issues involved here have been recently explored and set forth by Ingebretsen[6].

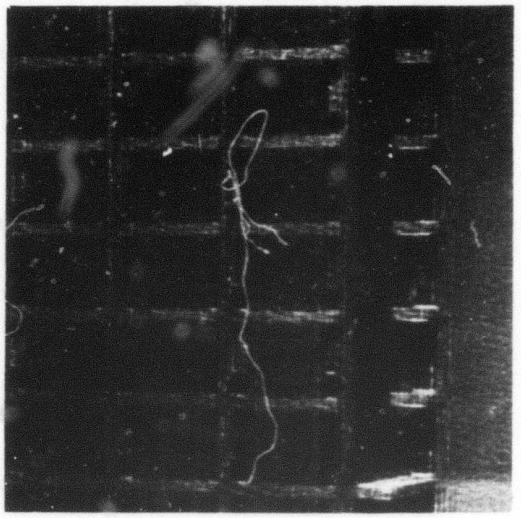

Figure A-1

A restoration of the office building using only two averaged sections to estimate the power spectrum.

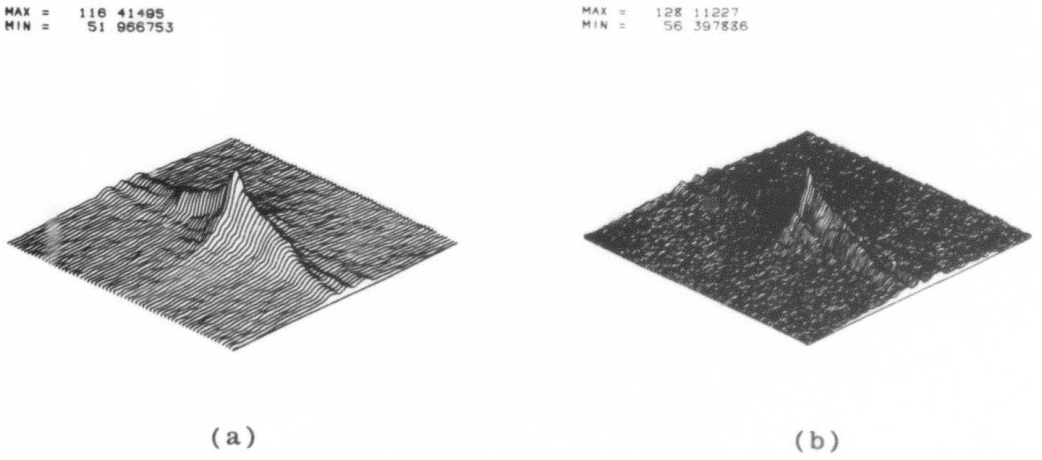

Figure A-2

(a) The power spectrum of a motion-blurred image.
(b) The same power spectrum computed on a doubly-fine grid.

(a)

MAX = 118 30577
MIN = 51 716226

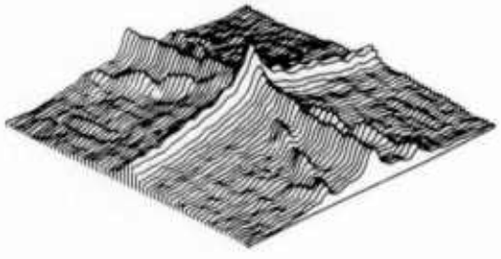

(b)

MAX = 115 03008
MIN = 47 74.678

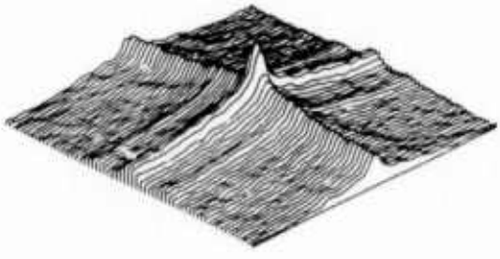

(c)

Figure A-3

(a) An original scene.
(b) The estimated power spectrum
(c) The average log spectrum.

APPENDIX B

Computation Times

One of the advantages of the restoration methods set forth in this thesis is the modest amount of computation needed to realize a successful restoration. The work presented in this dissertation was done on the University of Utah PDP-10 TENEX time sharing system and PDP-10 10/40 "single user" computer. These machines have fetch, floating multiply, and floating add times of approximately 2.5, 5, and 11 microseconds respectively.

The times associated with the three basic steps in the restoration process are tabulated below. The times given are for a 512x512 image, a 64x64 power spectrum, and a 64x64 restoration kernel. The time given for power spectrum estimation is for the averaging of 50 sections.

Power Spectrum Estimation (50 sections)	3 min
Blur Identification and Kernel Generation . . .	1 min
Two-Dimensional Convolution	15 min
Total	19 min

Appendix C

Notes on Blur Detection and Phase Generation Algorithms

Section 2.3 presented the notion of determining the blur by means of the transform of the log power spectrum, which was termed the power cepstrum. Only 20 sections need be averaged in order to estimate a power spectrum, which, when transformed to the cepstrum, contains sufficient information to detect the blur.

The power spectrum is, of course, windowed before it is Fourier transformed to the cepstral domain. A Parzen window was found to be very favorable as far as shaping the cepstral spikes for accurate identification by algorithm.

The blur identification algorithm is straightforward and heuristic. The algorithm attempts to identify motion blur by checking to see if the 10 most negative points all lie within a circle of radius 2.5. If it does not find this, it then looks for focus blur by checking to see if the most negative point and any one of the 20 other most negative points lie the same distance from the origin. If this is also not the case, the algorithm defaults to turbulence blur. The rationale behind the decision rules can easily be seen by examining the cepstra in Figures 2.5 and 2.9. The algorithm has been tested

without failure on the power cepstra of over 20 blurred images. The test consisted of comparing the results of the power cepstrum technique with those of the zero croesing method.

To generate the appropriate phase from the point spread function of the blur, a knowledge of the spacing of its zeroes in the frequency domain is needed. The case of motion blur is quite straightforward. A PSF of length α results in zero crossings $1/\alpha$ apart, the first one being at $f=1/\alpha$. Using a discrete Fourier transform of length N, the position of the first zero is then $K/N=1/\alpha$, or $K=N/\alpha$.

The caee of out-of-focue blur is only slightly more difficult. Ae ie shown in Appendix D, the Fourier transform of a cylinder of radiue R is $J_1(rR)/(rR)$. It is known[11] that the first zero occurs at $rR = 3.83$, hence,

$$2\pi fR = 2\pi(K/N)R = 3.83 \qquad \text{(C-1)}$$

$$K = 3.83\ N/(2\pi R) \qquad \text{(C-2)}$$

After R ie found from the power cepstrum, K can be calculated from equation C-2. K can also be found directly via the zero crossing technique of eection 2.2. The next five zero crossings occur at 7.01, 10.2, 13.3, 16.5, and 19.6.

Appendix D

Derivations

D-1 Minimum Mean Square Error Filter

In lieu of the volumes of material that have been written on Wiener filtering, the following two-page derivation is presented. Representing Diagram 3 mathematically, we have:

$$e = \int\int ([i(x,y) \circledast a(x,y) + n(x,y)] \circledast h(x,y) - i(x,y)]^2 dxdy$$

Parsevals's Theorm allows us to write this in the frequency domain:

$$e = \int\int ([I(f) \cdot A(f) + N(f)]H(f) - I(f))^2 df$$

Instead of minimizing e itself, we choose to minimize E{e}, which can be accomplished by minimizing the expected value of the above integrand. Assuming the noise to be uncorrelated to the signal, we can write:

$$E(I^2(f)[A(f)H(f)-1]^2 + [N(f)H(f)]^2)$$

Or

$$P_I(f)|A(f)H(f)-1|^2 + P_N(f)|H(f)|^2$$

Setting the derivative of this (with respect to the real and imaginary parts of H(f)) equal to zero, we have:

$$2P_I(f)[A(f)H(f)-1]A^*(f) + 2P_N(f)H(f) = 0$$

Or, finally:

$$H(f) = P_I(f)A^*(f)/[P_I(f)A(f)A^*(f) + P_N(f)]$$

$$H(f) = P_I(f)A^*(f)/[P_I(f)|A(f)|^2 + P_N(f)]$$

We have used two important relationships. The first being that if a(t) is the input to the system h(t), with b(t) the output, then

$$E(b^2(t)) = E\{[a(t) \circledast h(t)]^2\} = E\{A^2(f)H^2(f)\} = P_A(f)|H(f)|^2$$

The second relationship is the following: given three complex vectors, P, Q, R, where

$$P = |QR|^2$$

then the partial of P with respect to R is

$$2QRQ^* = 2|Q|^2R$$

This is easily shown by treating P as a sum, namely

$$P = Re(P) + jIm(P)$$

D-2 The Fourier Transform of a Cylinder

The two-dimensional Fourier transform of a function $f(x,y)$ is

$$F(u,v) = \int\int f(x,y)\exp[-j(ux+vy)]\,dx\,dy$$

Let: $f(x,y) = a$ for $x^2+y^2 \le R^2$, 0 elsewhere

Let: $x = \varsigma\cos(\theta)$

$y = \varsigma\sin(\theta)$

And: $u = r\cos(\Phi)$

$v = r\sin(\Phi)$

Then: $F(u,v) = \int\int a\cdot\exp[-jr\varsigma(\cos(\theta)\cos(\Phi) + \sin(\theta)\sin(\Phi))]\,\varsigma\,d\theta\,d\varsigma$

where the limits of integration are 0 to R and 0 to 2π.

This reduces to:

$$F(r,\Phi) = a\int\varsigma\int\exp[-jr\varsigma\cos(\theta-\Phi)]\,d\theta$$

$$F(r) = 2a\int\varsigma\pi I_0(-jr\varsigma)\,d\varsigma = 2a\pi\int J_0(r\varsigma)\varsigma\,d\varsigma$$

Substituting x for $r\varsigma$,

$$= 2\pi a/r^2\int xJ_0(x)\,dx$$

where the limits of integration are 0 to Rr.

Finally: $F(r) = 2\pi a/rJ_1(Rr)$

If we let the cylinder have unity volume, i.e. $\pi R^2 a = 1$, then

$$F(r) = 2J_1(Rr)/(Rr)$$

D-3 The Fourier Transform of $EXP(-x^2)$

$$G(f) = \int \exp(-x^2)\exp(-jx2\pi f)\,dx$$

$$G(f) = \int \exp[-(x^2+jx2\pi f)]\,dx$$

Completing the square, we have:

$$G(f) = \int \exp[-(x+j2\pi f/2)^2-(2\pi f/2)^2]\,dx$$

$$G(f) = \exp[-(2\pi f/2)^2] \int \exp[-(x+j2\pi f/2)^2]\,dx$$

A moment's contemplation will convince the reader that the value of the above integral is independent of f, nence

$$G(f) = k\cdot\exp[-(\pi f/2)^2]$$

D-4 The Fourier Transform of a Rectangle

Let: $g(x) = b$ for $-a \leq x \leq a$, 0 elsewhere.

$$G(f) = \int b \cdot \exp[-j2\pi ft]dt$$

where the limits of integration are from -a to a.

$$G(f) = -jb\int \sin(2\pi ft)dt + b\int \cos(2\pi ft)dt$$

The first integral is equal to zero; the value of the second is

$$G(f) = (b/2\pi f)[\sin(2\pi af) - \sin(-2\pi af)]$$

$$G(f) = (b/\pi f)\sin(2\pi af)$$

$$G(f) = 2ab\sin(2\pi af)/(2\pi af)$$

For a rectangle of unit area, i.e., b=1/2a, we have simply

$$G(f) = \sin(2\pi af)/(2\pi af)$$

List of References

[1] E.A. Guillemin, Theory of Linear Physical Systems, New York, N.Y.: Wiley, 1963.

[2] B. Gold and C.M. Radar, Digital Processing of Signals, New York, N.Y.: McGraw Hill, 1969.

[3] J.W. Goodman, Introduction to Fourier Optics, San Francisco: McGraw Hill, 1968.

[4] E.R. Cole, Homomorphic Filtering, thesis, University of Utah, 1973. Also ARPA technical report UTEC-CSc-74-029.

[5] B.L. McGlamery, "Image Restoration Techniques Applied to Astronomical Photography", in Astronomical Use of Television-type Image Sensors", report No. N71-28509-525 of the National Technical Information Service of the U.S. Dept. of Commerce, 1971.

[6] T.G. Stockham, T.M. Cannon, R.B. Ingebretsen, "The Digital Recording and Processing of Audio Signals", Proc. IEEE, April, 1975.

[7] B. Bogart, M. Healy, J. Tukey, "The Quefrency Analysis of Time Series for Echoes", Proc. Symp. on Time Series Analysis, M. Roeenblatt, Ed., New York, N.Y.: Wiley, 1963, ch 15.

[8] Personnal communication with Rafael Rom, Computer Science Department, Univereity of Utah.

[9] P.D.Welch, "The Use of the Fast Fourier Transform for the Estimation of Power Spectra", IEEE Trans. Audio Electroacoust, vol AU-15, pp. 70-73, June 1967.

[10] A.A. Sawchuk, "Space-Varient Image Motion Degradation and Restoration," Proc. IEEE, vol. 60, No. 7, pp. 854-861, July 1972.

[11] Wateon, A Treatise on the Theory of Bessel Functione", 2d ed, London: Cambridge University Press, 1944.

[12] Unpublished work by the author and T.G. Stockham, Jr.

[13] W. Lukosz, "Uebertragung Nicht-negativer Signale durch Lineare Filter", Optical Acta, Vol 9, 1962.

[14] R.P. Boas, Jr. and M. Kac, "Inequalities for Fourier Transforms of Positive Functions", Duke Math Journal, Vol. 12, 1945.

[15] A.V. Oppenheim, et.al. "Nonlinear Filtering of Multiplied and Convolved Signals", Proc. IEEE, Vol. 56, No. 8, August, 1968.

[16] J.W. Tukey, Exploratory Data Analysis, Vol. 3, Addison-Wesley, 1971 (limited preliminary edition).

[17] J.L. Horner, "Optical Restoration using Optimal Filter Theory of Images Blurred by Atmospheric Turbulence", in "Evaluation of Motion-Degraded Images", report SP-193, National Aeronautics and Space Administration, p 105, Washington, D.C., 1969.

[18] T.G. Stockham, "Restoration of Old Acoustic Recordings and Photographic Image Deblurring by Means of Digital Signal Processing", 1972 IEEE Intercon Digest, 72CH0581-9IEEE

[19] T.G. Stockham, "Restoration of Old Acoustic Recordings by Means of Digital Signal Processing", Audio Engineering Society Preprint No. 831.

[20] H.C. Andrews, "Positive Digital Image Restoration Techniques -- A Survey", Rerort No. ATR-73(8193)-2 of The Aerospace Corporation

ACKNOWLEDGEMENTS

I express my appreciation to Dr. Thomas G. Stockham, Jr., whose previous work in homomorphic filtering laid the foundation for this research.

I also thank Raphael Rom, whose many contributions influenced this work greatly.

The photographic reproductions shown in this report were made possible through the efforts of Michael Milochik.